**Title**
Nanoparticle-Based Induced Cre Recombination for Tissue-Specific Ischemia Targeting



**Author**
Chen, Cheng-Han

**Publication Date**
2015

Peer reviewed|Thesis/dissertation

UNIVERSITY OF CALIFORNIA

Los Angeles

# Nanoparticle-Based Induced Cre Recombination for Tissue-Specific Ischemia Targeting

A dissertation submitted in partial satisfaction of the requirements for the degree Doctor of Philosophy in Bioengineering

by

Cheng-Han Chen

2015

ABSTRACT OF THE DISSERTATION

Nanoparticle-Based Induced Cre Recombination

for Tissue-Specific Ischemia Targeting

by

Cheng-Han Chen

Doctor of Philosophy in Bioengineering

University of California, Los Angeles, 2015

Professor Benjamin M. Wu, Chair

Despite significant improvements in cardiac care over the past 50 years, ischemic heart disease continues to be the leading cause of morbidity and mortality worldwide. While therapies such as percutaneous coronary intervention have greatly improved reperfusion rates in acute myocardial infarction, effective therapies for the prevention and treatment of ischemia-reperfusion injury remain lacking. Some of the causes for this may include certain technical limitations of drug therapy, such as poor bioavailability, which can potentially be addressed through use of nanoparticle-based targeted drug delivery. This thesis evaluates the use of a nanoparticle-based induced Cre system in the development of nanoparticles for ischemia targeting and drug delivery. PLGA/4-Hydroxytamoxifen nanoparticles were fabricated using an emulsion-solvent evaporation method. These nanoparticles were then demonstrated to successfully induce gene

recombination in Rosa26-CreER x tdTomato and Rosa26-CreER x Rainbow transgenic mouse models both *in vitro* and *in vivo*, through direct intracellular delivery of 4-Hydroxytamoxifen to specific tissues. In addition, tissue specificity of gene recombination was enhanced through attachment of targeting antibodies such as CD31 and CD11b to the nanoparticles. Using this system, the uptake and drug delivery of nanoparticles to cardiac tissue subjected to ischemia-reperfusion injury was studied. Nanoparticle uptake and resultant drug delivery was found to be increased in areas of injury, and this uptake could be further increased by nanoparticle targeting of macrophages in the injury region. Control of vascular permeability through the administration of histamine was also found to influence nanoparticle uptake in certain organs. This research provides a framework for further studies to develop a nanoparticle-based system for delivery of targeted therapeutics for ischemia-reperfusion injury.

The dissertation of Cheng-Han Chen is approved.

Reza Ardehali

James C.Y. Dunn

Linda L. Demer

Benjamin M. Wu, Committee Chair

University of California, Los Angeles

2015

## DEDICATION PAGE

This dissertation is dedicated to my beautiful wife Victoria and my wonderful daughter Evelyn.

## TABLE OF CONTENTS

## LIST OF FIGURES

## LIST OF ACRONYMS

| | |
|---|---|
| Ab | Antibody |
| ACE-Inhibitors | Angiotensin-converting enzyme inhibitors |
| CABG | Coronary artery bypass graft |
| CreER | Cre recombinase – mutated estrogen receptor |
| DAPI | 4′,6-diamidino-2-phenylindole |
| DCM | Dichloromethane |
| DMEM | Dulbecco's Modified Eagle Medium |
| $ddH_20$ | Double distilled water |
| EC | Endothelial cell |
| EDC | 1-Ethyl-3-(3-dimethylaminopropyl)-carbodiimide |
| EPR | Enhanced permeability and retention |
| ER | Estrogen receptor |
| FACS | Flow assisted cell sorting |
| FBS | Fetal bovine serum |
| GFP | Green fluorescent protein |
| GRAS | Generally regarded as safe |
| IP | Intraperitoneal |
| IV | Intravenous |
| H&E | Hematoxylin and Eosin |
| HPLC-MS | High performance liquid chromatography - mass spectrometry |
| LAD | Left anterior descending artery |
| LV | Left ventricle |

| | |
|---|---|
| MES | 2-(N-morpholino)ethanesulfonic acid |
| MI | Myocardial infarction |
| NP | Nanoparticles |
| OH-Tam | 4-Hydroxytamoxifen |
| PBS | Phosphate buffered saline |
| PCI | Percutaneous coronary intervention |
| PDGFR-α | Platelet-derived growth factor receptor alpha |
| Pen/Strep | Penicillin-Streptomycin |
| PCL | Poly(caprolactone) |
| PLA | Poly(lactic) acid |
| PLGA | Poly(lactic-co-glycolic) acid |
| PVA | Poly(vinyl alcohol) |
| SDS | Sodium dodecyl sulfate |
| SEM | Scanning electron microscopy |
| SIRPA | Signal-regulatory protein alpha |
| Sulfo-NHS | N-hydroxysulfosuccinimide |
| tdT | tandem dimer Tomato |
| US | Ultrasound |
| UV | Ultraviolet |

## ACKNOWLEDGEMENTS

I would like to thank my advisor Dr. Benjamin Wu for the opportunity to work in his lab. He has set up such a dynamic multi-disciplinary environment with many interesting tools and approaches.

I would like to thank Dr. Reza Ardehali for the opportunity to work in his lab, his dedication to rigorous science, and his generosity with his resources. I would also like to think him for always being very supportive of my career as a physician-scientist and for many rounds of important career planning advice.

I would like to thank Dr. Linda Demer for being such a caring and supportive director of the STAR training program, to which I owe this terrific research and learning opportunity.

I would like to thank Dr. James Dunn and Professor Min Lee for their frequent valuable feedback during our regular research meetings.

Thank you to all of my labmates in the Wu, Ardehali, Dunn, and Lee labs for your help, support, feedback, and fun times.

Finally, thank you to my wife Victoria and daughter Evelyn for always reminding me what life is really about.

## VITA

| | |
|---|---|
| 2000 | S.B. Materials Science and Engineering<br>Massachusetts Institute of Technology |
| 2001 | S.M. Materials Science and Engineering<br>Massachusetts Institute of Technology |
| 2001-2004 | Research and Development Engineer<br>Medtronic, Inc.<br>Santa Rosa, California |
| 2008 | M.D.<br>University of California, San Diego School of Medicine |
| 2008-2009 | Intern in Internal Medicine<br>University of California, Los Angeles Medical Center |
| 2009-2010 | Resident in Internal Medicine<br>University of California, Los Angeles Medical Center |
| 2010-2015 | Fellow in Cardiovascular Disease<br>University of California, Los Angeles Medical Center |

# CHAPTER ONE - BACKGROUND

## 1.1 MOTIVATION

Ischemic heart disease (in the form of acute myocardial infarction and resultant ischemic cardiomyopathy) remains the leading cause of morbidity and mortality worldwide [1]. Although substantial improvements have been made in cardiac care over the past decades especially in primary prevention, approximately 1 million myocardial infarctions still occur each year in the United States. The mainstay of clinical therapy for acute myocardial infarction is early and successful cardiac reperfusion through thrombolytic therapy, percutaneous coronary intervention (PCI), or coronary artery bypass grafting (CABG). However, the reperfusion itself of coronary blood flow after a period of ischemia then frequently results in a pathological injury to the at-risk myocardium, termed ischemia-reperfusion injury [2]. This injury can account for up to 50% of the size of a myocardial infarction. Many of those patients then go on to develop heart failure, which now affects over 5 million patients [3]. While medications such as β-blockers and ACE-Inhibitors can slow the decline in heart function, patients with end-stage heart failure frequently require complete or partial replacement of cardiac function with either heart transplant or a mechanical assist device [4].

Over the years, many strategies have been developed and tested as potential therapies for ischemia-reperfusion injury [5]. However, none have yet to date been proven effective. Many explanations have been offered for the reason(s) successful animal studies have not yet translated into successful human clinical trials. Some of the reasons might involve technical factors such as poor therapeutic bioavailability that can potentially be addressed through bioengineering techniques such as targeted and controlled drug delivery. To address these shortcomings, this

project seeks to develop a nanoparticle-based drug delivery system for tissue-specific targeting of myocardium after ischemia-reperfusion injury.

## 1.2 REVIEW OF LITERATURE

### 1.2.1 Ischemic heart disease and ischemia-reperfusion injury

Ischemic heart disease is a condition characterized by reduced blood supply to the heart. This occurs due to blockages in the coronary arteries, which develop over decades of a person's life. A dreaded manifestation of ischemic heart disease is myocardial infarction (MI), frequently a result of acute plaque rupture of an unstable coronary artery lesion [6]. The most effective intervention for such an event is immediate coronary reperfusion either with thrombolytics [7], percutaneous coronary intervention [8], or occasionally coronary artery bypass graft surgery [9], all of which are of benefit in limiting the size of the infarction, preserving left ventricular systolic function, and salvaging viable myocardium.

Paradoxically however, the process of reperfusing oxygenated blood to ischemic myocardium is itself potentially harmful, associated with a condition known as ischemia-reperfusion injury [2]. When ischemic, the deprivation of oxygen and nutrients to the myocardium sets off a chain of metabolic changes including disruption of oxidative phosphorylation leading to mitochondrial membrane depolarization, depletion of ATP, switch to anaerobic glycolysis resulting in buildup of lactate and decrease in pH, and intracellular overload of $Ca^{2+}$. With sudden restoration of blood flow, the biochemical mileau again rapidly changes, causing oxidative stress, worsening of intracellular $Ca^{2+}$ overload, overly rapid correction of pH, and abundance of inflammatory mediators. These stressors eventually lead to cardiac cell death and loss of cardiac function,

resulting in a limitation in the amount of myocardium that was salvaged by the reperfusion intervention.

Many strategies have been considered for “cardioprotection” of the myocardium at risk of ischemia-reperfusion injury, including ischemic conditioning, therapeutic hyperoxemia and hypothermia. The most studied category has been pharmacologic agents for prevention and treatment of ischemia-reperfusion injury. Ranging from anti-inflammatory agents, to cyclosporine, to adenosine, to mitochondrial membrane stabilizers, they all share the feature that none have yet been proven to be effective in clinical trials [5]. Possible reasons include inappropriate pre-clinical testing, to premature testing of therapies inconclusive in animal studies, to in appropriate animal models, to poor clinical trial design. This continues however to be an area of active ongoing research, and multiple clinical trials are currently investigating novel agents as adjuncts to PCI for treating myocardial perfusion injury.

### 1.2.2 Nanoparticles and targeted drug delivery

Nanoparticles, originally in the form of liposomes and soon thereafter composed of polymeric materials, have been investigated as a vehicle for controlled drug delivery and release since the 1960’s [10]. Since then, the most commonly used materials for controlled drug release technologies have been the biodegradable polymers poly(lactic-co-glycolic) acid (PLGA), poly(lactic) acid, and poly(caprolactone) (PCL) (Figure 1-1). These formulations release encapsulated drug through a combination of hydrolysis of the polymer matrix (both surface and bulk) as well as diffuse of the drug out of the nanoparticle. The release kinetics will vary greatly based on the specific chemical properties of the polymer as well as its original processing characteristics [11].

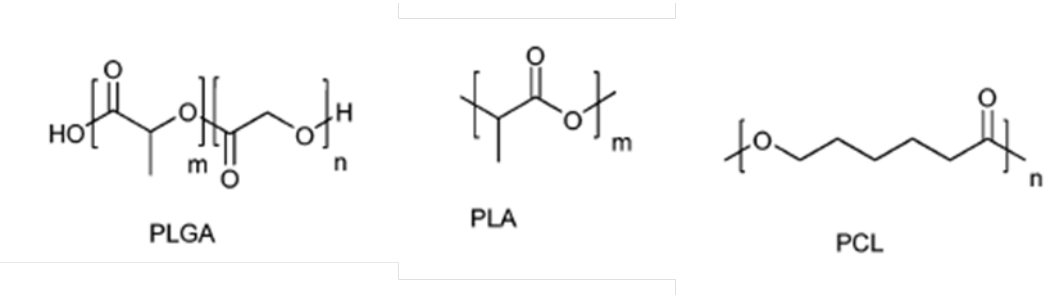


Figure 1-1: Common polymers used in nanoparticle drug delivery vehicles

A major attraction of the use of a PLGA-based composition is its biocompatibility. As the constituent building blocks of PLGA are monomoers of lactic acid and glycolic acid, its degradation products are therefore physiological molecules naturally processed during the citric acid cycle. Due to this, PLGA has been the most studied polymer for use in controlled drug release systems, has been FDA approved in multiple drug delivery formulations, and is considered by the FDA to be "generally regarded as safe" (GRAS). Specifically in nanoparticulate form, multiple formulations with various therapeutic payloads have been studied, without suggestion of toxicity [12,13].

Targeted therapy of drugs has been a major area of research in the field of pharmacology [14]. An injectable formulation able to be administered intravenously through a peripheral vein, and selectively target a certain organ or tissue, would have tremendous applications in medicine. Targeting strategies have typically been either "passive" in nature or "active". Passive targeting refers to an observation made by Maeda [15] that macromolecules of a certain size range tended to accumulate preferentially in tumor interstitium. Now a mainstay of targeted cancer therapeutic design, this "enhanced permeability and retention" (EPR) effect is known to be due to a combination of "leaky" tumor blood vessels and poor lymphatic drainage of the tumor.

Active targeting involves using ligands attached to the surface of nanoparticles in order to facilitate binding and uptake by specific cell types. The most commonly studied targeting ligand has been the antibody, although proteins, peptides nucleic acids, and sugars have also been attempted as well. As an active targeting strategy relies on interaction with their target to function, a passive component of nanoparticle delivery needs to be utilized as well to maximize the potential interactions between the nanoparticle and its target.

The very few studies which have investigated targeting of cardiac tissue have relied on an approach of antibody targeting of exposed intracellular proteins during cardiac injury [16,17]. However, these studies have generally looked at targeting of cells using attached antibodies, rather than therapeutic delivery of nanoparticles. One study utilized liposomes conjugated to an antibody to angiotensin II receptor thought to be up-regulated in the infarcted heart, and reported increased delivery to the infarcted heart after *in vivo* injection [18]. Clearly much more research needs to be performed in this area to develop a capability to actively deliver nanoparticle-based therapeutics to cardiac tissue.

### 1.2.3 CreER/LoxP induced gene recombination

The CreER/LoxP induced gene recombination transgenic system is a form (based on the original Cre-Lox technology) of site-specific recombinase technology widely used today in molecular biology to perform either deletions, insertions, translocations, or inversions at specific sites in the DNA of cells [19]. There are two important components of the system. The CreER is a Cre recombinase enzyme mutated to fuse to the estrogen receptor (ER). In its inactive state, it is localized to the cytosol by Hsp90. However, when its' agonists estrogen or tamoxifen bind, Hsp90 is released, and the ER shuttles the Cre to the nucleus. The second component of the

system is a segment of DNA flanked (“floxed”) by loxP sequences. When the Cre enters the nucleus, it then splices the loxP sites, causing recombination of the segment of DNA between the loxP sites [20].

Expression of the CreER fusion protein can be controlled either by a ubiquitous promoter or a tissue-specific promoter, thereby providing spatio-temporal control of gene expression. However, generation of tissue-specific strains remains a labor-intensive and expensive process. A targeted nanoparticle system based on targeted tamoxifen delivery to specific tissues, combined with a ubiquitous promoter CreER system, could obviate the need to develop tissue-specific mouse strains. This could potentially provide significant improvements to the cost and speed of biomedical research.

## 1.3 RESEARCH OBJECTIVES AND SPECIFIC AIMS

The overarching objective of this dissertation is to develop a nanoparticle-based drug delivery system for specific targeting of tissue ischemia, using the CreER/LoxP transgenic mouse platform. Specific aims are delineated as follows:

SPECIFIC AIM 1

Determine and improve tissue-specificity of nanoparticle-based CreER-mediated gene recombination

Specific Aim 1.1: Develop and characterize PLGA-based tamoxifen nanoparticles

Specific Aim 1.2: Induce gene recombination using tamoxifen nanoparticles in vitro and in vivo

Specific Aim 1.3: Increase tissue-specific nanoparticle-based gene recombination

SPECIFIC AIM 2

Determine and modify factors which influence nanoparticle accumulation in ischemic myocardium

Specific Aim 2.1: Determine nanoparticle accumulation under ischemic conditions

Specific Aim 2.2: Increase nanoparticle accumulation in ischemic myocardium with epitope targeting

Specific Aim 2.3: Induce increased NP delivery through control of vascular permeability

# CHAPTER 2: NANOPARTICLES FOR TARGETED INDUCED CRE RECOMBINATION

## 2.1 INTRODUCTION

Nanoparticles have long been studied as a method for targeted as well as controlled drug delivery. In order to develop a drug delivery platform for the targeted delivery of therapeutics to ischemic myocardium, we must first create a reliable model to evaluate and refine nanoparticle design and performance. Methods to directly track nanoparticle targeting and distribution rely on imaging techniques such as fluorescence microscopy, optical imaging, or magnetic resonance imaging. However, they rarely address the success of drug delivery itself. The induced Cre/loxP system has been a powerful tool in developmental and molecular biology through its ability to temporally control gene recombination through the administration of the drug tamoxifen, and spatially control gene recombination through selective design of mouse strains in which the CreER gene is under the control of ubiquitous vs. tissue-specific promoters. It is hypothesized that this system can be used as a reporter system for drug delivery by nanoparticles if the encapsulated drug was 4-Hydroxytamoxifen (the active form of tamoxifen), and the CreER gene left under the control of a ubiquitous promotor. In this scenario, both temporal and spatial control of gene recombination would be governed by the intracellular uptake of nanoparticles delivering the OH-Tam, resulting in expression of a reporter gene specifically if drug delivery were successful. Modifications in nanoparticle design could then be analyzed for their effects on reporter gene expression.

This chapter of the dissertation establishes the experimental methods and results that demonstrate the use of OH-Tam loaded nanoparticles for targeted induced Cre recombination.

## 2.2 MATERIALS AND METHODS

### Materials

Poly(lactic-co-glycolic) acid (50:50) (PLGA 50:50) ($M_w$ 7,000-17,000, Cat#719897) , Poly(lactic-co-glycolic) acid (85:15) (PLGA 85:15) ($M_w$ 50,000-75,000, Cat#430471), Poly(vinyl alcohol) (PVA) ($M_w$ 31,000-50,000, Cat# 363073), 4-Hydroxytamoxifen (OH-Tam) (Cat# H7904), Coumarin 6 (Cat# 442631), Sodium dodecyl sulfate (98%, Cat# 862010), Nunc Lab-Tek 2-well chamber slide system (Cat# C6682), Methanol (≥99.9%, for HPLC, Cat# 34860), EDC (Cat# 39391), and Sulfo-NHS (Cat# 56485), were obtained from Sigma-Aldrich (St. Louis, MO).

Dichloromethane (DCM) (Cat# D1511), Dulbecco's Modified Eagle Medium w/ 4.5g/L glucose, L-glutamine & sodium pyruvate (DMEM 1X, Cellgro, Cat # 10-013-CV), fetal bovine serum (FBS, Cat# MT35015CV), 70μm nylon meshes (Cat# 22363548), BCA Protein Assay Kit (Cat# PI-23227), anti-CD31 Ab (clone 2H8, Cat# EN-MA3105), anti-CD3e Ab (clone 145-2C11, Cat# PIMA517655), and Gibco ACK Lysing Buffer (Cat# A10492), were obtained from Fisher Scientific (Waltham, MA).

Acetonitrile (Cat# 9017-33) was obtained from Thomas Scientific (Swedesboro, NJ)

Medium 199 (Cat# 11150-059), and AlexaFluor 647-conjugated anti-rabbit Ab (Cat# A-31573) were obtained from Life Technologies (Grand Island, NY).

Liberase TM (Cat# 05401127001) was obtained from Roche (Indianapolis, IN).

Poly(L-lactide) acid (PLA) (IV 0.90-1.20 Cat#B6002-2) was obtained from Lactel (Birmingham, AL).

Anti-CD11b Ab (Cat# 553308), and AlexaFluor 647-conjugated anti-CD11b Ab (Cat# 557686) was obtained from BD Biosciences (Franklin Lakes, NJ)

Anti-CD31 Ab (Cat# ab2364) was obtained from Abcam (Cambridge, United Kingdom).

Fabrication and characterization of 4-Hydroxytamoxifen-loaded nanoparticles

Nanoparticles encapsulating 4-Hydroxytamoxifen were created using an emulsion-solvent evaporation technique. Three different carrier polymers were used: Poly(lactic-co-glycolic) acid (PLGA) (50:50), PLGA (85:15), and Poly(L-lactide) acid (PLA). Briefly, the "oil" phase of the emulsion was prepared by mixing 50mg of the polymer of interest, 4mg of 4-Hydroxytamoxifen, and 0.5mg of Coumarin 6 in 3ml of dichloromethane for 2 hours. 2ml of this solution was then slowly poured into 8ml of cold 1% PVA (in $ddH_20$) solution. This solution was then sonicated on ice using a Fisher Scientific Model 500 ultrasonic dismembrator, with a microtip probe at 30% output for 120 seconds. The emulsion was then stirred overnight (minimum of 12 hours) with a magnetic stir-bar at 700rpm to allow the organic solvent to evaporate. The resulting nanoparticles were washed of the PVA surfactant by 2 successive rinses in $ddH_20$ (solution centrifugation at 14.5k rpm for 8 minutes followed by sonication of the pellet at 10% output for 10 seconds). With the final rinse, the nanoparticles were resuspended in $ddH_20$ at the desired concentration, frozen at -80ºC for 24 hours, and lyophilized for 48 hours with the Labconco FreeZone 4.5. As controls for some of the experiments, nanoparticles without 4-Hydroxytamoxifen were also fabricated as per the above procedure.

Lyophlized nanoparticles were imaged under scanning electron microscopy using a Nova Nano SEM 230, with low vacuum detector, 5.0 to 10.0 keV accelerating voltage, and 2.0 to 3.0 spot

size. Of note, gold sputter coating was not performed as this was found in preliminary experiments to distort the structure of the nanoparticles.

To determine nanoparticle size and surface zeta-potential, lyophilized samples were suspended in solution which was placed in a cuvette (Malvern DTS0012) and inserted into a Zetasizer Nano ZS (Malvern, Worchestershire, UK) where the zeta-size, polydispersity index, and zeta-potential of triplicate samples was determined. The Zetasizer measures nanoparticle zeta-size by dynamic light scattering and zeta-potential by the electrophoretic mobility of the particles, which is then related to the potential using the Smoluchowski approximation. Numerical results are presented as a zeta-average size or a zeta-potential ± standard deviation.

4-Hydroxytamoxifen elution from the prepared nanoparticles was measured by preparing 1 mg/ml suspensions of lyophilized nanoparticles in 0.5% SDS/PBS. At the specified time points of 1 hour, 24 hours, and 72, hours, the suspensions were centrifuged at 14.5k rpm for 8 minutes, and supernatant collected. The UV absorbance of the supernatant at 280nm was then analyzed and quantified using a Tecan Infinite 200 plate reader (Tecan, Männedorf, Switzerland). Concentration of 4-Hydroxytamoxifen in the supernatant was determined by relating the absorbance with a generated standard curve. All experimental samples were generated in triplicate.

*In vitro* uptake of OH-Tam-loaded nanoparticles

The *in vitro* uptake of OH-Tam-loaded nanoparticles into cells was studied by incubating nanoparticles with cultured murine dermal fibroblasts. Briefly, ear biopsies of wild-type C57BL/6 mice were performed, cut into small pieces, and digested with Liberase Blendzyme TH and TM in Medium 199 plus DNase I and polaxamer at 37ºC for 1 hour. Cells were passed

through a 70 μm cell strainer and centrifuged. The cells were resuspended in culture media (DMEM with 10% FBS and 1% Pen/Strep), and plated on 2-well chamber slides. After the cells were cultured to approximately 60-70% confluence, PLGA(50:50) nanoparticles were suspended in culture media at the experimental concentrations (1 μg/ml, 10 μg/ml, 100 μg/ml, and 1000 μg/ml). For each condition, the nanoparticle/culture media suspension was incubated with the cells for either 1 hour or 12 hours. At the end of the incubation, the media was aspirated from the chamber, and the cells were fixed by first washing with cold PBS x 3, followed by cold 4% paraformaldehyde for 15 minutes, followed by repeat cold PBS rinse x 3. VectaShield DAPI mounting medium was then placed on each slide, and the slide was sealed with a coverslip. Imaging was performed under fluorescence microscopy (AF6000LX, Leica Microsystems, Wetzlar, Germany) as well as confocal microscopy (TCS SP5-STED, Leica Microsystems, Wetzlar, Germany).

*In vivo* biodistribution of OH-Tam-loaded nanoparticles

The *in vivo* biodistribution of OH-Tam-loaded nanoparticles was studied by intravenous injection of generated nanoparticles into C57BL/6 wild-type mice. Briefly, PLGA(50:50) nanoparticles were created as described above. The lyophilized nanoparticles were then suspended in PBS at a concentration of 1 mg/ml. The suspension was filtered through a 0.22 μm sterile filter. For each mouse, 200 μl of the nanoparticle suspension was injected in a lateral tail vein with a 29G hubless needle, and allowed to circulate for 2 hours. The mice were then euthanized by cervical dislocation after anesthesia with 5% isoflurane. For each mouse, the heart, one lung, one kidney, the liver, the spleen, and the brain were harvested. The organs were then fixed in 4% paraformaldehyde overnight at 4ºC, followed by dehydration with sucrose solution for 24 hours. The organs were then mounted in OCT embedding compound, and frozen

at -80ºC for 48 hours. Sections of 6-8μm thick tissue were then cut with a cryostat, and mounted on standard histological slides. Imaging was then performed under fluorescence microscopy (AF6000LX, Leica Microsystems, Wetzlar, Germany) as well as confocal microscopy (TCS SP5-STED, Leica Microsystems, Wetzlar, Germany).

Generation of transgenic mice

$Rosa26^{CreER};tdT^{F/F}$ mouse lines were obtained by crossing Rosa26-CreER mice with lineage reporter R26R-tdTomato mice. $Rosa26^{CreER};R26^{VT2/GK3}$ mouse lines were obtained by crossing Rosa26-CreER mice with the multicolor reporter R26-"Rainbow" mice. All mice were on a C57BL/6 background.

All animal experiments were performed in accordance with policies established by the UCLA Chancellor's animal research committee as well as U.S. National Institute of Health guidelines.

OH-Tam induced CreER recombination *in vitro*

Induction of CreER-mediated recombination was studied *in vitro* in dermal fibroblasts from both the $Rosa26^{CreER};tdT^{F/F}$ and the $Rosa26^{CreER};R26^{VT2/GK3}$ transgenic mice models. Briefly, the ear biopsies from mice from each transgenic model were performed, cut into small pieces, and digested with Liberase Blendzyme TH and TM in Medium 199 plus DNase I and polaxamer at 37ºC for 1 hour. Cells were passed through a 70 μm cell strainer and centrifuged. The cells were resuspended in culture media (DMEM with 10% FBS and 1% Pen/Strep), and plated on 2-well chamber slides. After the cells were cultured to approximately 60-70% confluence, PLGA(50:50) nanoparticles (containing OH-Tam and Coumarin 6 as previously described) were suspended in culture media at 100 μg/ml, and the nanoparticle/culture media suspension was incubated with the cells for 24 hours. As controls, cells were also incubated with: a) no

nanoparticles, b) nanoparticles lacking 4-Hydroxytamoxifen, and c) free 4-Hydroxytamoxifen at a concentration of 100nM. All experimental conditions were run in triplicate. At the end of the 24 hour incubation, the media was aspirated from the chamber, and the cells were fixed by first washing with cold PBS x 3, followed by cold 4% paraformaldehyde for 15 minutes, followed by repeat cold PBS rinse x 3. VectaShield DAPI mounting medium was then placed on each slide, and the slide was sealed with a coverslip. Imaging was performed under fluorescence microscopy (AF6000LX, Leica Microsystems, Wetzlar, Germany), with 5 20x images recorded for each experimental condition. Quantification of cells in each image was performed using ImageJ image processing and analysis software (NIH). Numerical results are presented as a percentage of positive to total cells in field of view ± standard deviation. Statistical testing was performed using the Student's t-test, and statistical significance was achieved with a two-sided *P* value $\leq 0.05$.

Serum detection of OH-Tam

To study the bloodstream release of 4-Hydroxytamoxifen from its carrier nanoparticles, serum quantification was performed using a capillary high-performance liquid chromatography/tandem mass spectrometry (HPLC-MS) method. Briefly, OH-Tam nanoparticles were generated as described above, injected (400 μg) into the lateral tail vein of wild-type C57BL/6 mice, and allowed to circulate for either 1 hour, 12 hours, and 5 days. As a control, other mice were injected with 1mg 4-Hydroxytamoxifen (dissolved in corn oil) with standard intraperitoneal technique, which was then allowed to circulate for 12 hours. At the end of the specified time points, blood from each mouse was collected through retro-orbital capillary collection. The blood was allowed to clot, and then centrifuged at 4ºC for 8 minutes at 15K rpm. The serum supernatant was removed, and then further processed as follows for HPLC. 40μl of serum from

each mouse was mixed with 80 µl of acetonitrile, vortexed, and then centrifuged at 14.5k for 8 minutes. The supernatant was removed, and then dried under a gentle argon stream. The resulting residue was then resuspended in 40µl of100% methanol, vortexed for 1 minute, and centrifuged at 14.5k for 8 minutes. The supernatant was then removed, and 4-hydroxytamoxifen measured as previously described [21], with the following modifications: a 3- µl aliquot of sample was injected into a C18 analytical column, maintained at 40ºC, eluted with a 5-95% B gradient over 5 minutes at 400 µl/min, where solution A was aqueous formic acid (0.3%) and solution B was acetonitrile. The column effluent was monitored by tandem mass spectrometry (MS/MS) detection of the transition m/z 388.2→71.9 using a Waters LCT Premier UPLC/MS system. The area under the curve of the peak at a retention time of 2.37 minutes was quantified, and the concentration of 4-Hydroxytamoxifen was calculated using a generated standard curve. Numerical results are presented as nanograms of OH-Tam per mL of blood ± standard deviation.

OH-Tam induced CreER recombination *in vivo*

The tissue distribution of induced CreER-mediated recombination was studied *in vivo* in both the $Rosa26^{CreER}$;$tdT^{F/F}$ and the $Rosa26^{CreER}$;$R26^{VT2/GK3}$ transgenic mice models. Briefly, OH-Tam nanoparticles were generated as described above. Nanoparticles without OH-Tam were also generated for use as a control. For each condition, 1mg (200 µg for 5 consecutive days) of nanoparticles were injected into the lateral tail vein of each mouse, for both the $Rosa26^{CreER}$;$tdT^{F/F}$ and the $Rosa26^{CreER}$;$R26^{VT2/GK3}$ transgenic mouse models, and allowed to circulate for a total of 6 days (counting from the first injection). As a control, other mice were injected with 1mg 4-Hydroxytamoxifen (dissolved in corn oil) on day 1 with standard intraperitoneal technique, and then no more OH-Tam was given for the remainder of the 6 days. The mice were then euthanized by cervical dislocation after anesthesia with 5% isoflurane.

Heparin was injected prior to anesthesia to prevent coagulation of blood in the coronary arteries. For each mouse, the heart, one lung, one kidney, the liver, and the spleen, were harvested. The organs were then fixed in 4% paraformaldehyde overnight at 4ºC, followed by dehydration with sucrose solution for 24 hours. The organs were then mounted in OCT embedding compound, and frozen at -80ºC for 48 hours. Sections of 7-8μm thick tissue were then cut with a cryostat, and mounted on standard histological slides. Imaging was then performed under fluorescence microscopy (AF6000LX, Leica Microsystems, Wetzlar, Germany) as well as confocal microscopy (TCS SP5-STED, Leica Microsystems, Wetzlar, Germany).

Antibody conjugation to OH-Tam-loaded nanoparticles

To covalently conjugate antibodies onto the OH-Tam nanoparticle surface, carbodiimide chemistry utilizing EDC and sulfo-NHS. EDC was selected as it is well known to react with a carboxylic acid group (in our case the terminal end of the PLGA molecule) to form a highly reactive O-acylisourea intermediate. The addition of sulfo-NHS then leads to a stable amine-reactive sulfo-NHS ester, which then reacts with primary amines on the antibody to form a stable amide bond. For this study, conjugation of anti-CD3 Ab, anti-CD11b Ab, and anti-CD31 Ab to OH-Tam nanoparticles were all performed. Briefly, OH-Tam-loaded nanoparticles were prepared as described previously. The nanoparticles were activated by suspending in MES buffer (pH 6.0) at a concentration of 2mg/ml, to which 500 μg of EDC and 500 μg of sulfo-NHS was added. This mixture was kept at room temperature for 30 minutes. To remove unused reagents, 2 successive rinses in PBS were performed (solution centrifugation at 14.5k rpm for 8 minutes followed by sonication of the pellet at 10% output for 10 seconds). The final resuspension of the nanoparticles was into PBS. A control experiment was also performed in which EDC was withheld from the above steps, in order to examine antibody adsorption onto the nanoparticle

surface. Antibody conjugation to the activated nanoparticles was then performed by incubating 1mg of activated nanoparticles with 250 μg of the desired antibody for 6 hours. Excess antibody was then removed through 2 successive rinses in PBS were performed (solution centrifugation at 14.5k rpm for 8 minutes followed by sonication of the pellet at 10% output for 10 seconds).

Characterization of antibody-conjugated OH-Tam-loaded nanoparticles

The zeta-average size and zeta-potential of the nanoparticles were determined at multiple steps of the conjugation process of Anti-CD3 Ab to OH-Tam loaded nanoparticles: at baseline, after activation of the nanoparticles with EDC/sulfo-NHS, and after antibody conjugation. This was performed in triplicate at each condition with the Zetasizer Nano ZS as previously described.

In addition, the degree of antibody binding to nanoparticles was also studied using a protein quantitation assay. First, the antibody conjugation process was performed as described above to produce nanoparticles conjugated to Anti-cd3 Ab as well as nanoparticles conjugated to Anti-CD31. In order to determine the effect of the conjugation process itself on the degree of antibody bound to the nanoparticles, a control set of nanoparticles was created in which the entire conjugation process was followed except for the addition of EDC crosslinker. Nanoparticles created by these processes were then tested with the BCA Protein Assay Kit (Pierce), which is a colorimetric assay based on the known reduction of $Cu^{2+}$ to $Cu^{1+}$ by protein in a sample. Each sample was incubated with the assay working reagent for 30 minutes at 37ºC in the dark. The absorbance of each sample at 560nm was measured on a Tecan Infinite 200 plate reader (Tecan, Männedorf, Switzerland). Protein amount was then determined by comparing the result with that from a generated standard curve. To calculate the degree of antibody binding to nanoparticles (ratio of number of antibodies detected to the number of

nanoparticles), a theoretical antibody molecular weight of 150 kDa and a nanoparticle size of 200nm diameter (resulting in a calculation of 1.32275 E-13 moles of NP per mg) was used. All experimental samples were tested in triplicate. Numerical results are presented as number of antibody molecules per nanoparticle ± standard deviation.

In vivo targeting of anti-CD31 OH-Tam-loaded nanoparticles

Targeting of endothelial cells by anti-CD31 OH-Tam-loaded nanoparticles was studied in the $Rosa26^{CreER}$;$tdT^{F/F}$ transgenic mouse model. Briefly, anti-CD31-conjugated nanoparticles were prepared as described above. As a control, OH-Tam-loaded nanoparticles that did not undergo any antibody conjugation were also prepared. For each of these conditions, 500 μg of conjugated nanoparticles (250 μg for 2 consecutive days) were injected into the lateral tail vein of $Rosa26^{CreER}$;$tdT^{F/F}$ transgenic mice. Triplicates were performed of each condition. After 5 days, the mice were euthanized by cervical dislocation after anesthesia with 5% isoflurane. Heparin was injected prior to anesthesia to prevent coagulation of blood in the coronary arteries. For each mouse, the heart, one lung, one kidney, the liver, and the spleen, were harvested. The organs were then fixed in 4% paraformaldehyde overnight at 4ºC, followed by dehydration with sucrose solution for 24 hours. The organs were then mounted in OCT embedding compound, and frozen at -80ºC for 48 hours. Sections of 7-8μm thick tissue were then cut with a cryostat, and mounted on standard histological slides. Immunofluorescent staining on the frozen sections was performed using a primary antibody to CD31 (Abcam) and the appropriate AlexaFluor 647-conjugated secondary antibody (Life). Imaging was then performed under fluorescence microscopy (AF6000LX, Leica Microsystems, Wetzlar, Germany) as well as confocal microscopy (TCS SP5-STED, Leica Microsystems, Wetzlar, Germany).

In vivo targeting of anti-CD11b OH-Tam-loaded nanoparticles

Targeting of bloodstream monocytes and neutrophils by anti-CD11b OH-Tam-loaded nanoparticles was studied in the Rosa26$^{CreER}$;tdT$^{F/F}$ transgenic mouse model. Briefly, anti-CD11b-conjugated nanoparticles were prepared as described above. As a control, OH-Tam-loaded nanoparticles that did not undergo any antibody conjugation were also prepared. For each of these conditions, 900 μg of conjugated nanoparticles (300 μg for 3 consecutive days) were injected into the lateral tail vein of Rosa26$^{CreER}$;tdT$^{F/F}$ transgenic mice. Triplicates were performed of each condition. After the fourth day, the mice were injected with heparin, and blood from each mouse was collected through retro-orbital capillary collection. For each mouse, 500 μL of blood was mixed with 10 mL RBC lysing buffer at room temperature for 5 minutes. The mixture was then centrifuged at 300g for 5 minutes, the aspirate removed, and the cell pellet gently resuspended and washed with cold PBS. This was again centrifuged at 300g for 5 minutes. The pellet was resuspended in 200 μL FACS buffer containing 1:50 AlexaFluor 647-conjugated anti-CD11b Ab. The antibody was allowed to incubate for 30 minutes at room temperature in the dark, after which excess antibody was washed off by adding 3ml of PBS and centrifuging at 300g for 3 minutes. The cells were resuspended in FACS buffer for analysis. Samples were acquired on a FACSAria Cell Sorter (BD Biosciences), and data were analyzed with FlowJo software. Numerical results are presented as a percentage of tdTomato positive cells to CD11b positive cells in the analyzed samples ± standard deviation. Statistical testing was performed using the Student's t-test, and statistical significance was achieved with a two-sided *P* value $\leq 0.05$.

## 2.3 RESULTS

### Nanoparticle characterization

Nanoparticles composed of PLGA(50:50), PLGA(85:15), or PLA and encapsulating 4-Hydroxytamoxifen and Coumarin 6 were fabricated by the emulsion-solvent evaporation method. Characterization of the nanoparticles included evaluation of NP morphology, size, polydispersity, and drug elution properties. SEM (Figure 2-1) revealed that the NP were spherical in shape, and relatively monodisperse.

Zetasizer analysis (Figure 2-2) showed that all three formulations resulted in particle sizes in the range of 220 to 230 nm with polydispersity index ranging from 0.05 to 0.20. Zeta potential analysis of surface charge demonstrated that all three formulations resulted in a zeta potential of approximately -30 mV, in the range that would promote stable suspensions with lower risk of aggregation.

*In vitro* drug elution testing of all three formulations (Figure 2-3) demonstrated 3 distinct drug release patterns. The PLGA(50:50) nanoparticle formulations resulted in a rapid "burst" release of OH-Tam within the first hour, while the majority of the encapsulated drug released within 24 hours. Conversely, PLA nanoparticles control the release of encapsulated OH-Tam such that less than 10% is released within the first hour, and further release remains similarly slow. The drug elution behavior of PLGA(85:15) nanoparticles falls between these two extremes. These results are consistent with the known behavior of these materials as agents for controlled delivery of therapeutics [11].

Based on these results, and on the desired performance criteria for our drug delivery system, it was decided to focus choose the PLGA(50:50) formulation as the material of choice for the

nanoparticles. Chiefly, the requirement for the nanoparticle to quickly release its payload of OH-Tam into the cytoplasm of cells after cell uptake necessitates a drug elution curve with a quick "burst" release, such as that demonstrated by PLGA(50:50).

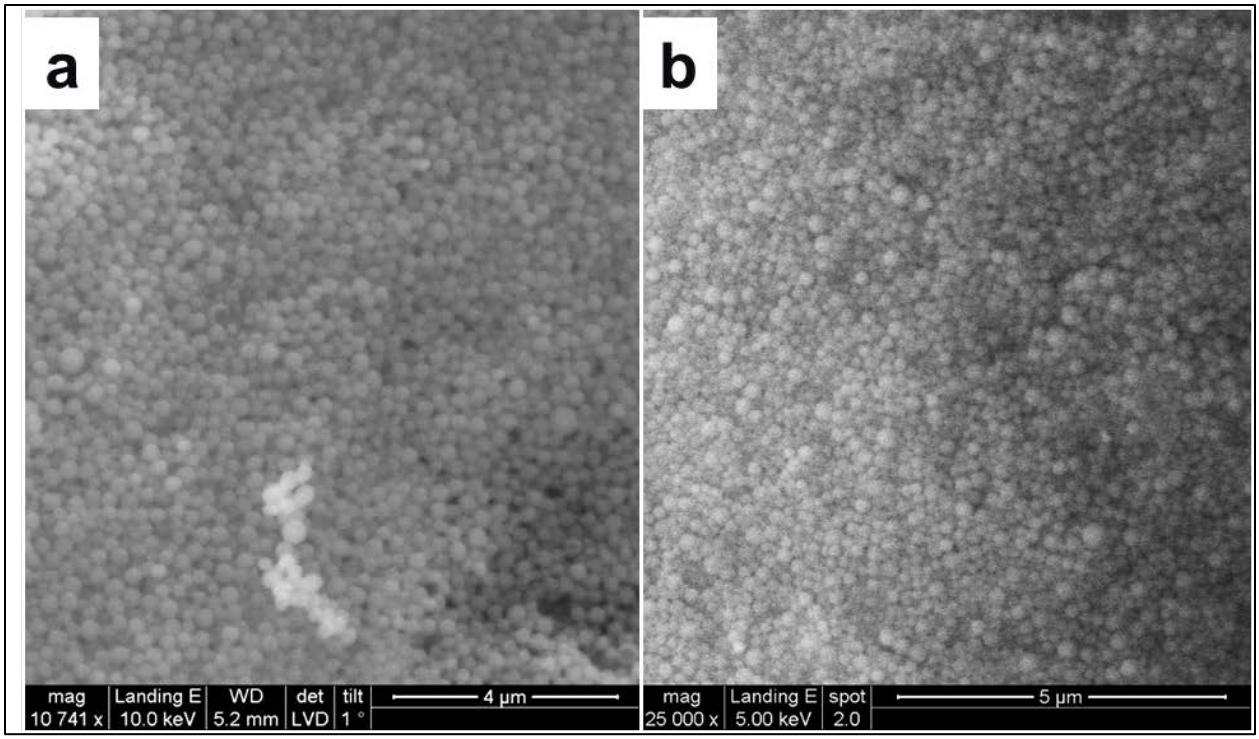


**Figure 2-1: Scanning electron microscopy of OH-Tam-loaded (a) PLGA(50:50) and (b) PLA nanoparticles created by the emulsion-solvent evaporation method.** Particles are spherical in morphology and monodisperse on gross examination.

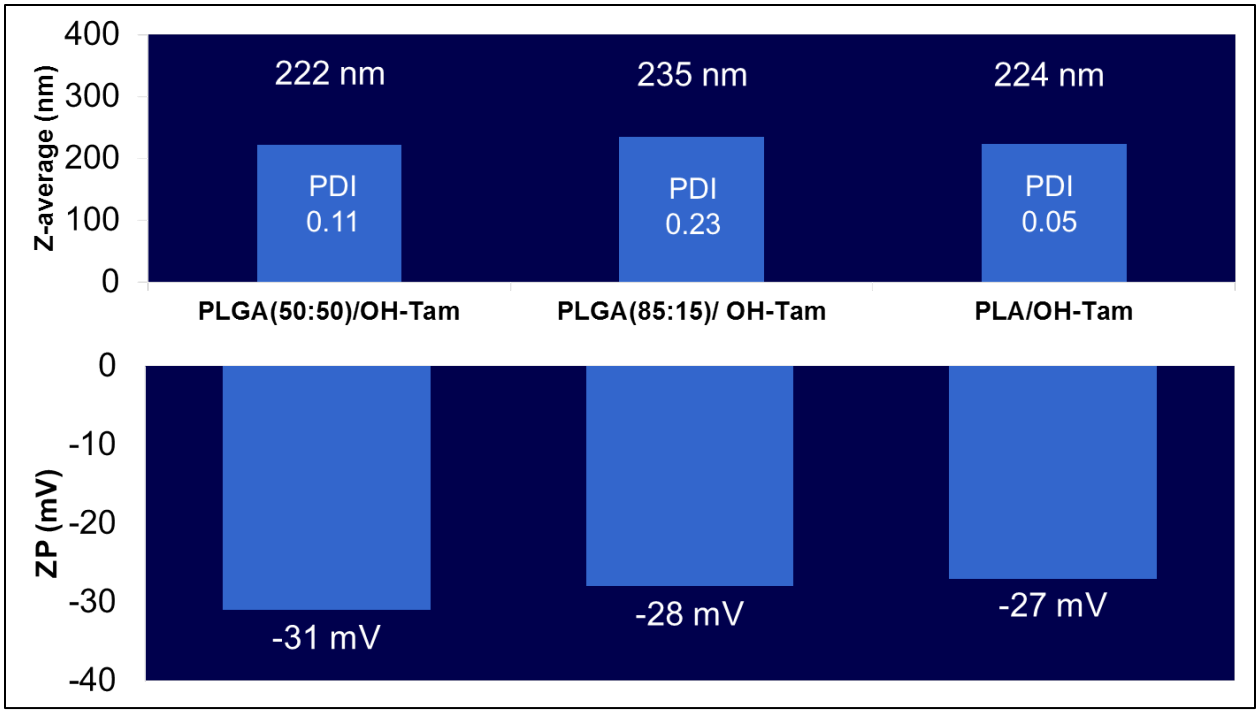


**Figure 2-2: Average particle size, polydispersity, and zeta-potential of OH-Tam-loaded PLGA(50:50), PLGA(85:15), and PLA nanoparticles.** All three formulations resulted in relatively monodisperse particle sizes in the range of 220 to 230 nanometers. Zeta-potentials are consistent between groups, and the negative potentials promote stable nanoparticle suspensions.

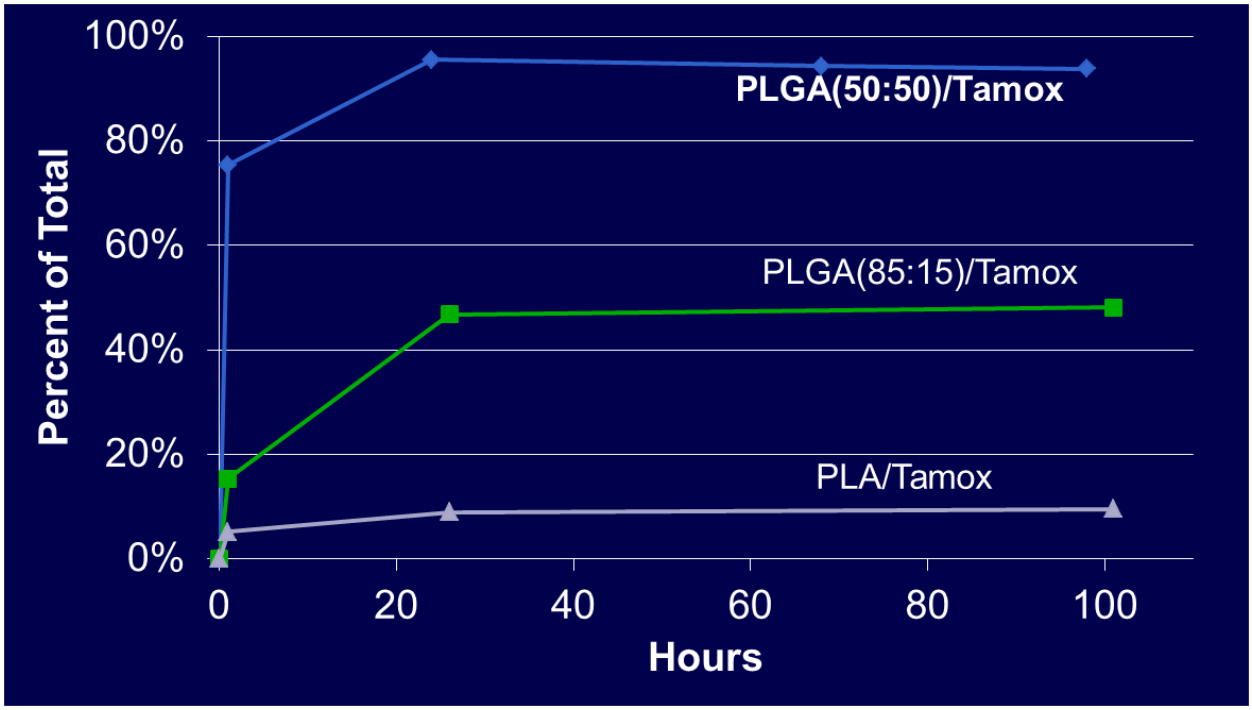


**Figure 2-3: Elution of OH-Tam from PLGA(50:50), PLGA(85:15), and PLA nanoparticles.** PLGA(50:50) nanoparticle formulations result in a rapid "burst" release of OH-Tam within the first hour, while the majority of the encapsulated drug released within 24 hours. Conversely, PLA nanoparticles control the release of encapsulated OH-Tam such that less than 10% is released within the first hour, and further release remains similarly slow.

*In vitro* uptake of OH-Tam-loaded nanoparticles

In this experiment (Figure 2-4) examining the ability of OH-Tam-loaded PLGA(50:50) nanoparticles to be adequately endocytosed by cells, multiple NP concentrations (ranging from 1 ug/ml to 1000 ug/ml) as well as 2 different incubation time points (1 hour and 2 hours) were studied. Nanoparticle uptake was evaluated by determining the relative level of fluorescence detected in the cell, as the encapsulated Coumarin 6 would theoretically be detectable in the GFP range. The fluorescence seen increased with nanoparticle concentration. However, it did not appear that incubation for 12 hours resulted in further nanoparticle uptake after 1 hour.

Cells from this study were then examined under Confocal microscopy (Figure 2-5), which again evaluated nanoparticle uptake into the cell by the basis of GFP signal detected. This demonstrated (most clearly seen in the z-stack cross-section) that the nanoparticles were clearly well distributed within the cells.

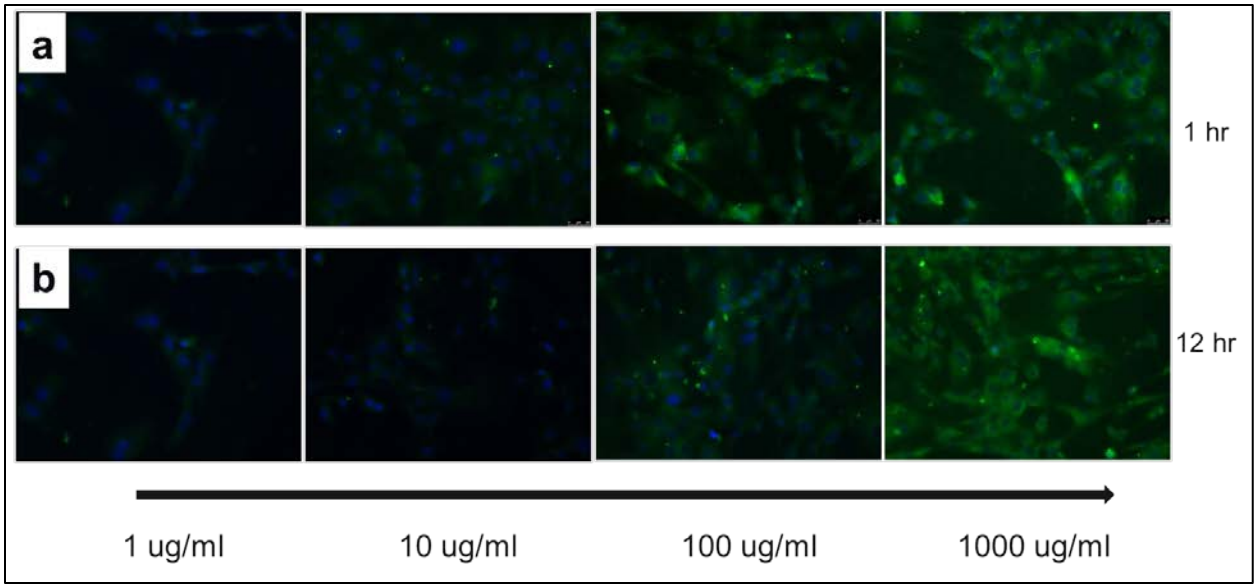


**Figure 2-4: Accumulation of nanoparticles within dermal fibroblasts *in vitro***. Fluorescence micrographs were taken after incubation for either (a) 1 hour or (b) 12 hours, at nanoparticle concentrations in culture media ranging from 1 ug/ml to 1000 ug/ml. There is clearly an increase in nanoparticle uptake with increased nanoparticle concentration, as evidenced by increase in fluorescence detected from the cells. The fluorescence detected results from signal from Coumarin 6 encapsulated within the nanoparticles. There is no visible difference in nanoparticle uptake after incubation for either 1 hour or 12 hours.

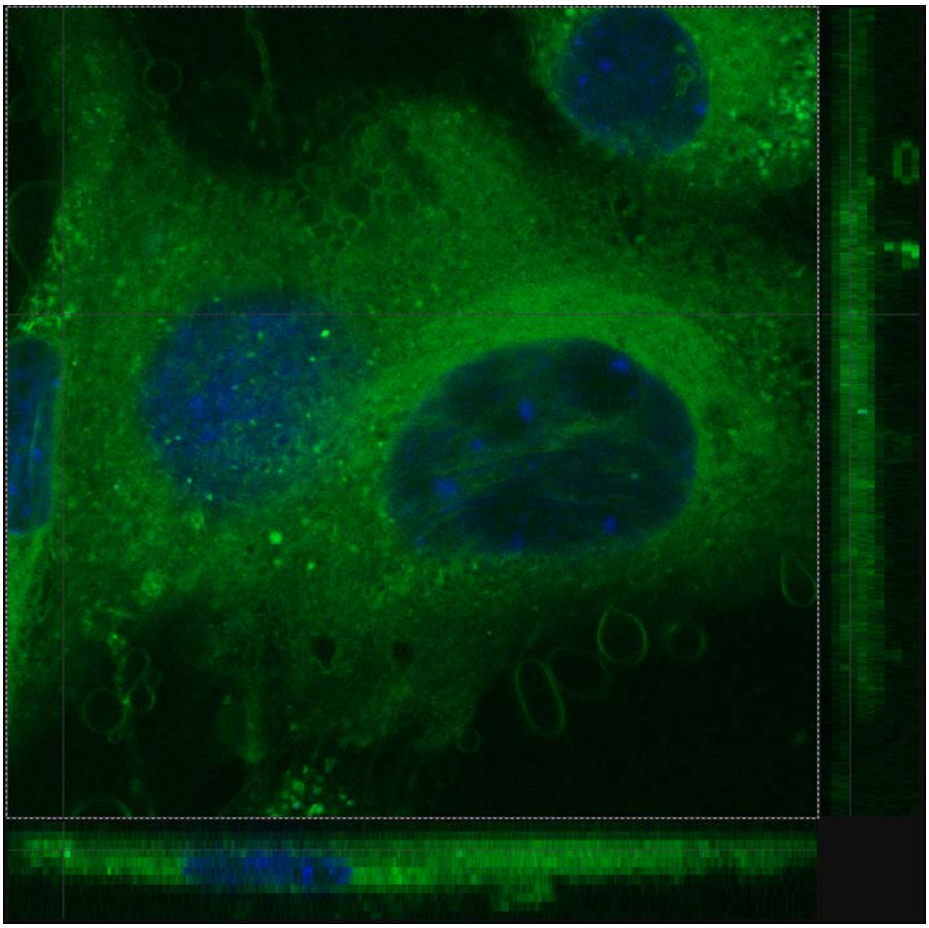

**Figure 2-5: Confocal microscopy of dermal fibroblasts after incubation with nanoparticles.** Representative cells chosen from sample incubated at a concentration of 1mg/ml nanoparticles for 12 hours. The nanoparticles (as evidenced by fluorescent signal from the encapsulated Coumarin 6) are clearly dispersed throughout the cytoplasm of the cells. This is most clearly seen in the z-stack cross-section.

*In vivo* biodistribution of OH-Tam-loaded nanoparticles

This experiment focused on the examining the biodistribution of OH-Tam PLGA(50:50) nanoparticles after lateral tail vein injection into mice. There is clear accumulation of nanoparticles within the liver and spleen sections, while there is no detectable nanoparticle uptake in either the heart, liver, kidney, or brain. This is consistent with the known function of the mononuclear phagocyte system of the liver and spleen in clearing the bloodstream of foreign particles.

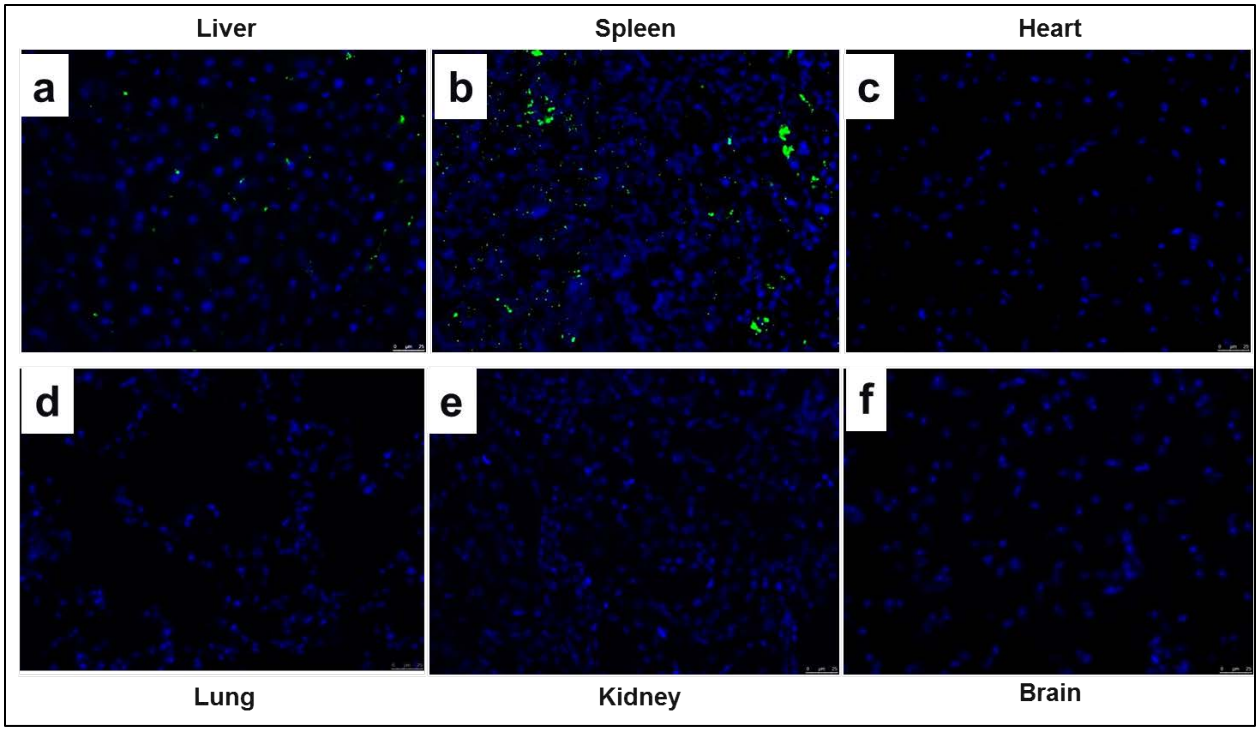


**Figure 2-6: Representative fluorescent micrographs of organ sections after PLGA(50:50) nanoparticle tail vein injection and circulation.** There is clear accumulation of nanoparticles within the liver and spleen sections, while there is no detectable nanoparticle uptake in either the heart, liver, kidney, or brain. This is consistent with the known function of the mononuclear phagocyte system of the liver and spleen in clearing the bloodstream of foreign particles.

OH-Tam induced CreER recombination *in vitro*

The first study (Figure 2-7) evaluated the ability of OH-Tam-loaded nanoparticles to induce recombination in Rosa26-CreERxtdTomato dermal fibroblasts. These nanoparticles induced recombination in the vast variety of cells in this model. The second study (Figure 2-8) evaluated the ability of OH-Tam-loaded nanoparticles to induce recombination in a more complicated induced Cre system (Rosa26-CreERxRainbow). Again, the majority of cells in this model did undergo recombination. However, it was noted that this model perhaps might be "leaky", as there was baseline expression of the reporter proteins (cerulean, mOrange, and mCherry) in the control samples which did not deliver any OH-Tam.

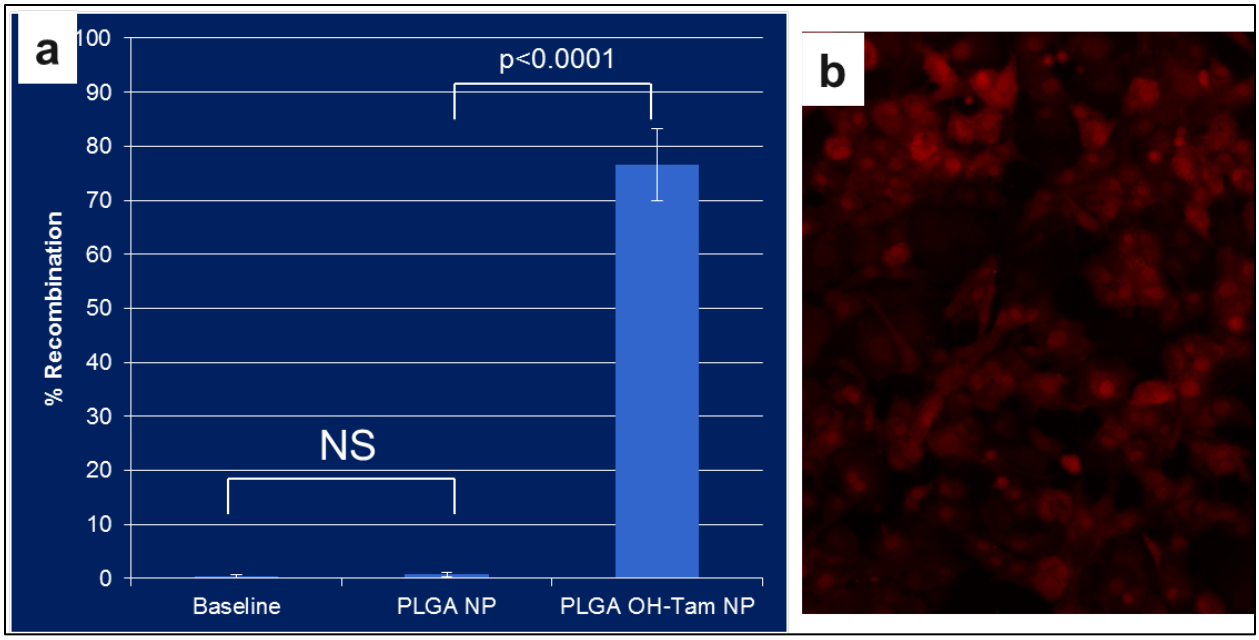


**Figure 2-7: PLGA NP-delivered OH-Tam induces CreER-tdTomato recombination *in vitro*.** Panel (a) shows the large number of recombined cells after incubation with PLGA(50:50) OH-Tam-loaded nanoparticles. Panel (b) shows fluorescence microscopy of the cells after expression of the tdTomato reporter protein.

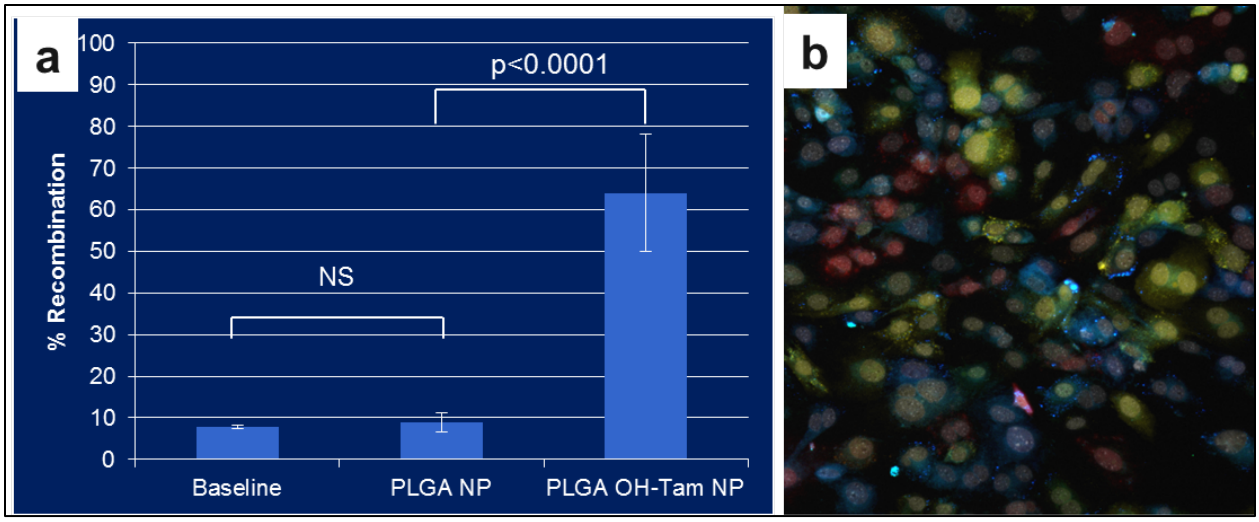


**Figure 2-8: PLGA NP-delivered OH-Tam induces CreER-Rainbow recombination *in vitro*.** Panel (a) shows the significant increase in recombined cells after incubation with PLGA(50:50) OH-Tam-loaded nanoparticles. Panel (b) shows fluorescence microscopy of the cells after expression of the cerulean, mOrange, and mhCerry reporter proteins.

Serum detection of OH-Tam

For the purposes of this nanoparticle application, it is imperative that there be minimal to no bloodstream release of OH-Tam prior to the nanoparticle reaching its cell destination. This would thus ensure that there would be targeted delivery to the cell of interest. In addition, released free OH-Tam may induce recombination in cells which had not taken up nanoparticles, resulting in false positive results in our experiments.

To determine the degree of bloodstream release of OH-Tam from PLGA(50:50) nanoparticles, blood from mice injected with IV nanoparticles as well as IP OH-Tam was evaluated by a HPLC-MS test method as previously described. Figure 2-9 shows a representative tracing of a standard sample of OH-Tam at a concentration of 10 ng/mL, demonstrating that a clear signal can be obtained even down to this low level.

While a bloodstream level of 300 ng/mL (Figure 2-10) could be detected in mice injected with IP free 4-Hydroxytamoxifen, those mice injected with PLGA(50:50) NP encapsulating OH-Tam which was allowed to circulate for either 1 hour, 12 hours, or 5 days all had non-detectable levels of OH-Tam in their blood. This indicates that no significant bloodstream release of OH-Tam occurs when the OH-Tam is packaged in nanoparticle form.

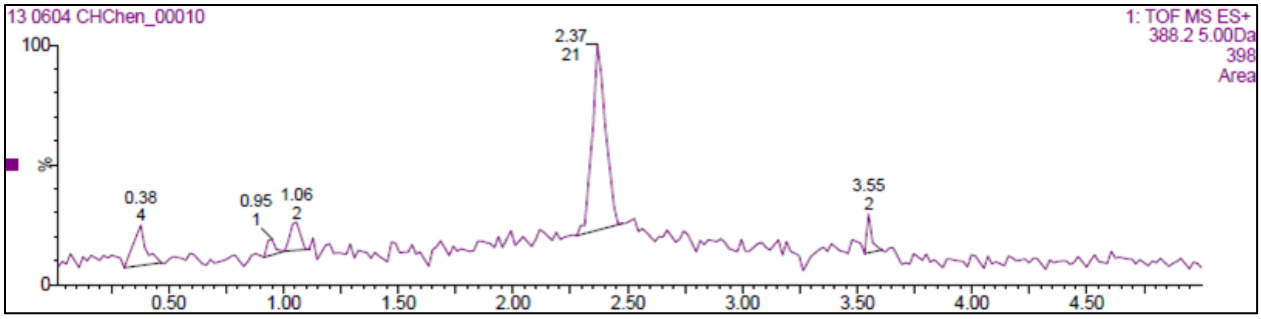


**Figure 2-9: HPLC-MS detection of 4-Hydroxytamoxifen**. Tracing is shows reliable detection of OH-Tam down to a serum level of 10 ng/mL. Transition m/z is 388.2, with peak at 2.37 minutes retention per the described test method.

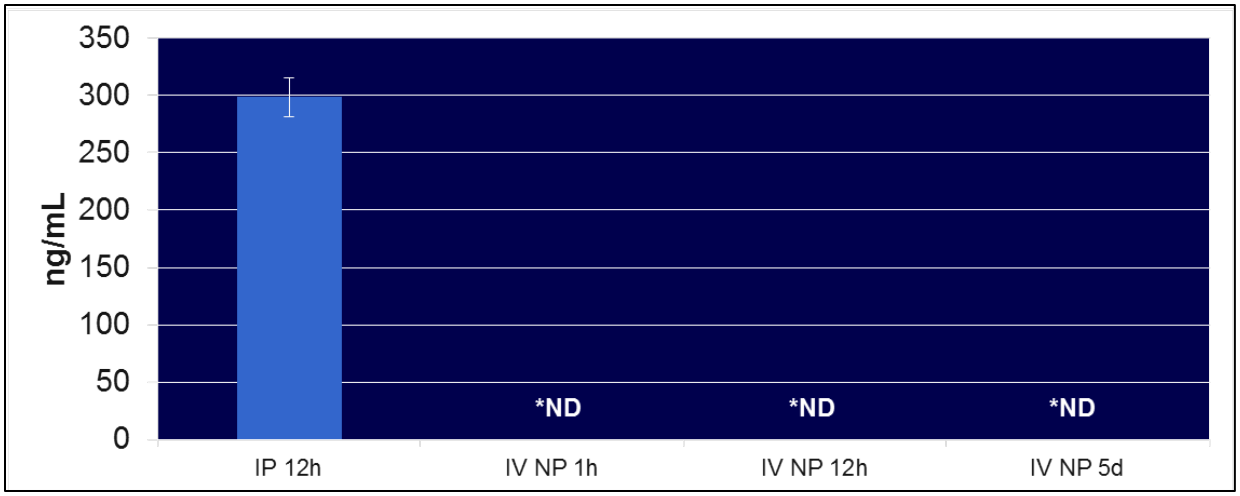


**Figure 2-10: Comparison of OH-Tam bloodstream levels between IP injection of OH-Tam and IV injection of OH-Tam encapsulated PLGA(50:50) nanoparticles.** While there is a clear bloodstream level of 4-Hydroxytamoxifen measured in the bloodstream 12 hours after intraperitoneal injection, no OH-Tam can be detected in the blood stream with IV injection of encapsulated OH-Tam when measured at 1 hour, 12 hours, and 5 days.

OH-Tam induced CreER recombination *in vivo*

Once it was established that OH-Tam-loaded nanoparticles could successfully induce recombination *in vitro*, and that no bloodstream release of the encapsulated drug occurs, it was decided to proceed to evaluation of the nanoparticle formulation ability to induce CreER recombination *in vivo*. The first study (Figure 2-11) compared the degree and pattern of induced CreER recombination (in the CreER-tdTomato transgenic system) after standard IP injection of 4-Hydroxytamoxifen with that from IV injection of OH-Tam-loaded PLGA(50:50) nanoparticles. The second study (Figure 2-13) examined the same premise but using the more complicated CreER-Rainbow transgenic system. In both systems, standard intraperitoneal injection of OH-Tam resulted in recombination and expression of fluorescent reporter protein(s) in a majority of cells in every organ examined. However, with IV injection of encapsulated OH-Tam, the vast majority of the detected recombination events occurs in the liver and the spleen, with very few to no recombination events occurring in the other organs. This is consistent with known nanoparticle clearance by mononuclear phagocyte system in the liver and spleen, resulting in organ specific delivery of encapsulated OH-Tam.

To further examine the question of whether recombination occurs from direct nanoparticle delivery of OH-Tam or possibly from release of OH-Tam into the bloodstream by nanoparticles prior to uptake into a cell, confocal microscopy was performed of multiple areas of positive recombination (Figure 2-12). These results show that nanoparticles co-localize to cells with tdTomato reporter gene expression, further supporting the claim that recombination is being driven by OH-Tam that has been directly carried to the cytoplasm of a cell by the nanoparticle.

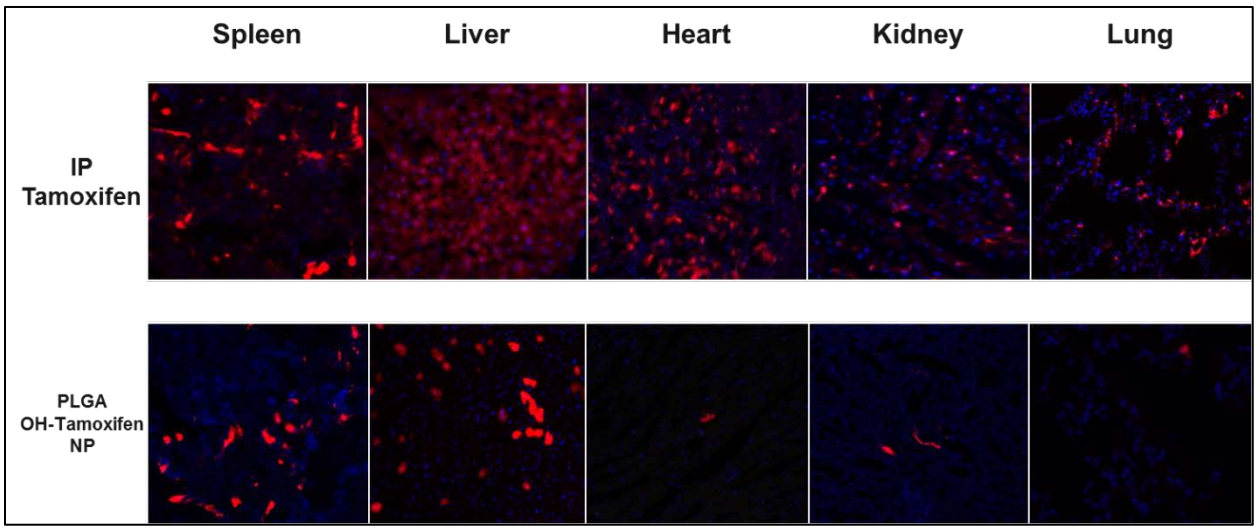


**Figure 2-11: Comparison of induced Cre recombination in the CreER-tdTomato system between IP injection of OH-Tam and IV injection of OH-Tam encapsulated PLGA(50:50) nanoparticles.** With the standard intraperitoneal injection of OH-Tam, recombination (resulting in expression of the tdTomato fluorescent reporter protein) occurs in a majority of cells in every organ examined. However, with IV injection of encapsulated OH-Tam, the vast majority of the detected recombination events occurs in the liver and the spleen, with very few to no recombination events occurring in the other organs. This is consistent with known nanoparticle clearance by the liver and spleen, resulting in organ specific delivery of encapsulated OH-Tam.

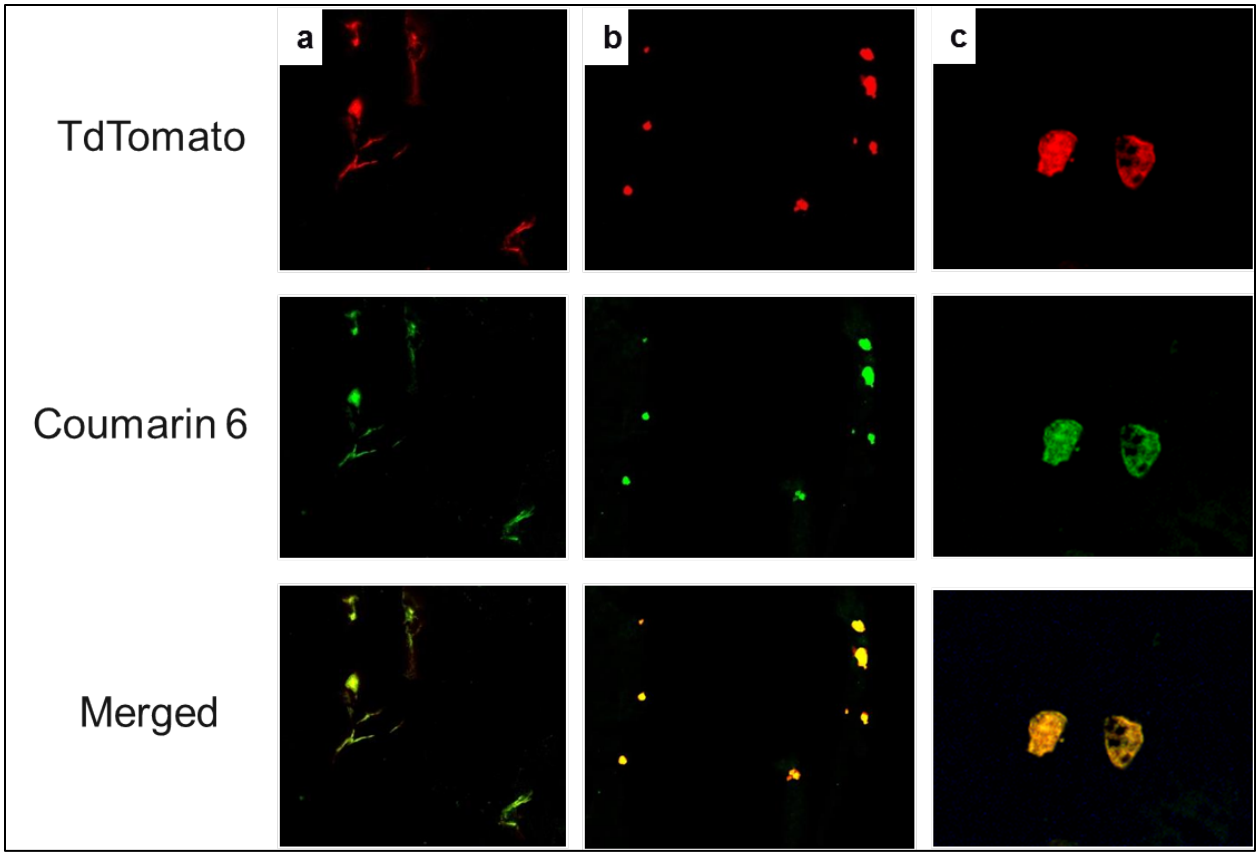


**Figure 2-12: Co-localization of CreER-induced tdTomato reporter gene expression and nanoparticle accumulation in individual cells.** These Confocal micrographs of representative tissue sections (labeled (a), (b), and (c)) from the liver reveal co-localization of nanoparticles (as evidenced by the encapsulated Coumarin 6 signal) with expression of tdTomato reporter gene (from CreEr-induced gene recombination after intracellular delivery of OH-Tam).

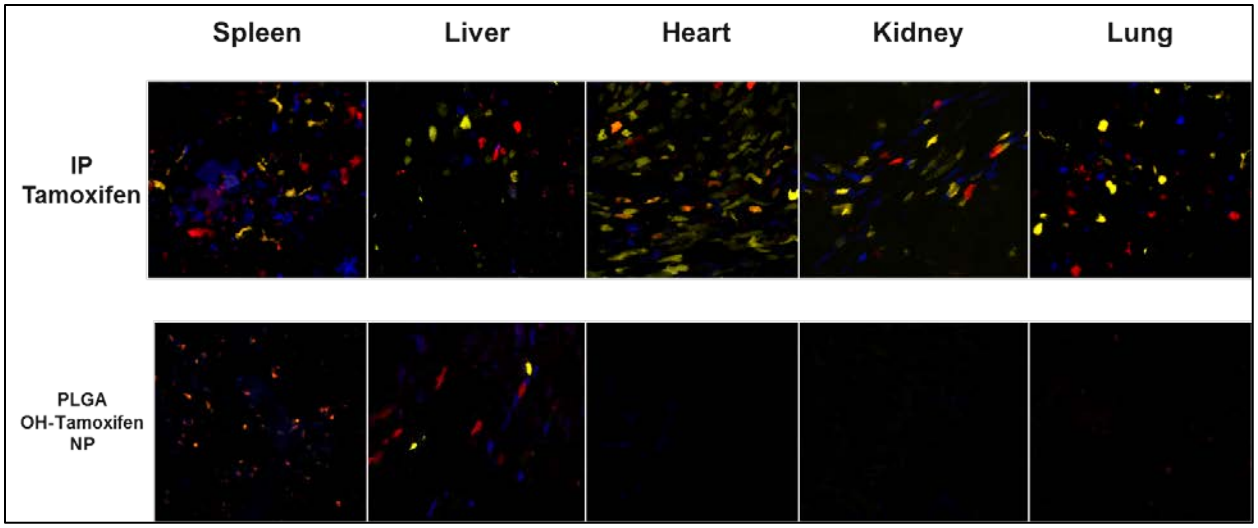


**Figure 2-13: Comparison of induced Cre recombination in the CreER-Rainbow system between IP injection of OH-Tam and IV injection of OH-Tam encapsulated PLGA(50:50) nanoparticles.** With the standard intraperitoneal injection of OH-Tam, recombination (resulting in expression of the fluorescent reporter proteins cerulean, mOrange, and mCherry) occurs in many cells in every organ examined. However, with IV injection of encapsulated OH-Tam, the vast majority of the detected recombination events occurs in the liver and the spleen, with very few to no recombination events occurring in the other organs. This is consistent with known nanoparticle clearance by the liver and spleen, resulting in organ specific delivery of encapsulated OH-Tam.

Characterization of antibody-conjugated OH-Tam-loaded nanoparticles

While the liver- and spleen- specific induced recombination seen after delivery of OH-Tam-loaded nanoparticles is a direct byproduct of natural particle clearing mechanisms in the organs of the mononuclear phagocyte system, true tissue specific control of recombination would necessitate modification of the nanoparticle design to include active targeting. Three different model antibodies were chosen for straightforward bloodstream path to their targets: CD31 (endothelial cells), CD11b (monocytes/macrophages/neutrophils), and CD3 (T-cells). Antibody conjugation through carbodiimide linker chemistry to the surface of the nanoparticles was felt to be a straightforward method to endow the NP with tissue targeting capabilities. Figure 2-14 below reports characterization of the nanoparticles during the conjugation process. It can be seen that the size of the nanoparticle steadily increases from a baseline of approximately 195nm, to approximately 242nm after antibodies have been bound to the surface. This size increase would be consistent with the averages size of an antibody. Regarding zeta potential, the initial zeta-potential measured was -24 mV. With the addition of the sulfo-NHS ester crosslinker, the zeta potential becomes much less negative, possibly due to shielding of the previously available carboxylic acid end-groups. After conjugation of the antibody, there is a return to a more negative surface potential as the surface charge becomes dependent on the specific amino acid composition of the antibody used.

Quantitation of the degree of antibody binding to the surface of a nanoparticle was also examined. The conjugation process was performed with and without the EDC crosslinker. It is apparent (Figure 2-15) that even in the absence of crosslinker, antibodies non-covalently bind to the surface of the nanoparticles (approximately 357 CD3 antibodies and 302 CD31 antibodies per PLGA nanoparticle). However, the addition of crosslinker almost doubles the amount of

antibody bound (to 666 CD3 antibodies and 726 CD31 antibodies per PLGA nanoparticle). It should be noted that the conjugation process results in an amide bond being produced with any free amine on the antibody surface, which may potentially be in the active site of the antibody. This would then result in shielding of the active site, rendering that antibody molecule inactive. However, given the large number of antibodies calculated to be bound to each nanoparticle, it is more than likely that each nanoparticle has more than 1 active antibody able to bind to its target.

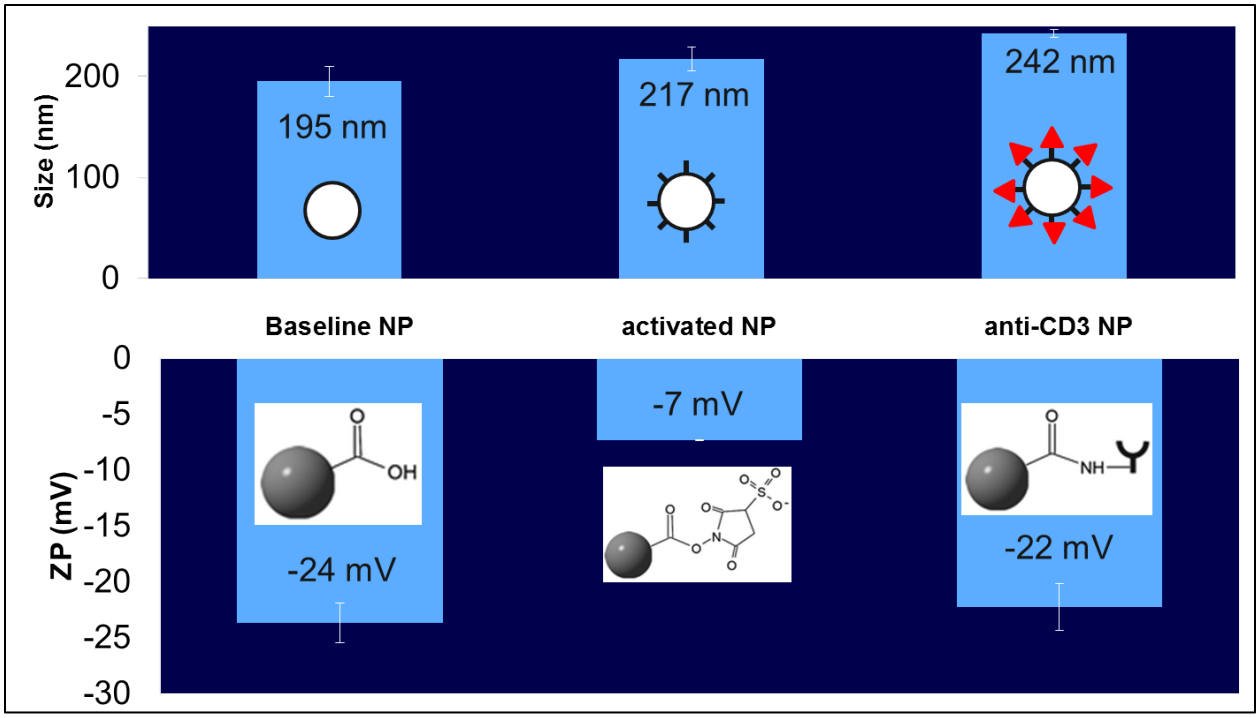


**Figure 2-14: Changes in size and surface potential of PLGA(50:50) nanoparticles with sequential surface modification during carbodiimide-mediated conjugation to antibodies.** At baseline, PLGA(50:50) OH-Tam-loaded nanoparticles are approximately 195nm in size, with a zeta-potental of -24 mV. With the addition of the sulfo-NHS ester crosslinker, particle size increases slightly, and the zeta potential becomes much less negative, possibly due to shielding of the previously available carboxylic acid end-groups. After conjugation of the antibody, average particle size has increased to approximately 242nm, consistent with the surface addition of an antibody approximately 15-20nm in size. This also results in a return to a more negative surface potential.

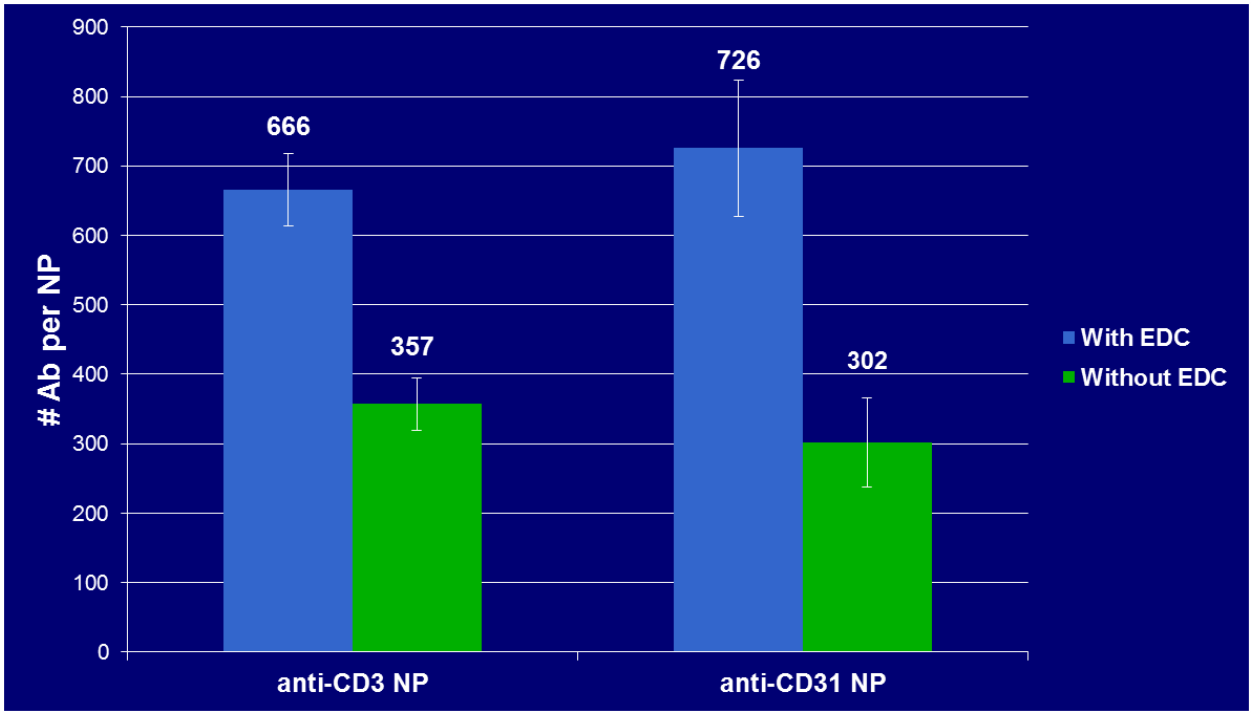


**Figure 2-15: Effect of chemical conjugation on the degree of protein binding to the surface of PLGA(50:50) nanoparticles.** This study examined and quantified the amount of antibody bound to the surface of nanoparticles for both the anti-CD3 and anti-CD31 antibody systems. The conjugation process was performed with and without the EDC crosslinker. It is apparent that even in the absence of crosslinker, antibodies non-covalently bind to the surface of the nanoparticles (approximately 357 CD3 antibodies and 302 CD31 antibodies per PLGA nanoparticle). However, the addition of crosslinker almost doubles the amount of antibody bound.

In vivo targeting of anti-CD31 OH-Tam-loaded nanoparticles

The ability for anti-CD31 OH-Tam-loaded nanoparticles to effect tissue-specific (endothelial cell) recombination was tested (Figure 2-16) in the CreER-tdTomato transgenic mouse model. IV injection of control nanoparticles (OH-Tam loaded nanoparticles without targeting antibody) resulted in the known pattern of recombination primarily in the liver and spleen parenchymal cells. However, with the addition of CD31 antibody to the surface of the nanoparticle, IV injection resulted in recombination in cells each different organ that appeared to resemble endothelial cells by morphology (Figure 2 bdf). This was further examined by staining the slides with CD31 antibody (abcam), and examining under Confocal microscopy (Figure 2-17). This revealed that the tdTomato positive cells co-localized with Coumarin 6, and indeed did stain positive for CD31, indicating successful targeting of endothelial cells by the nanoparticles.

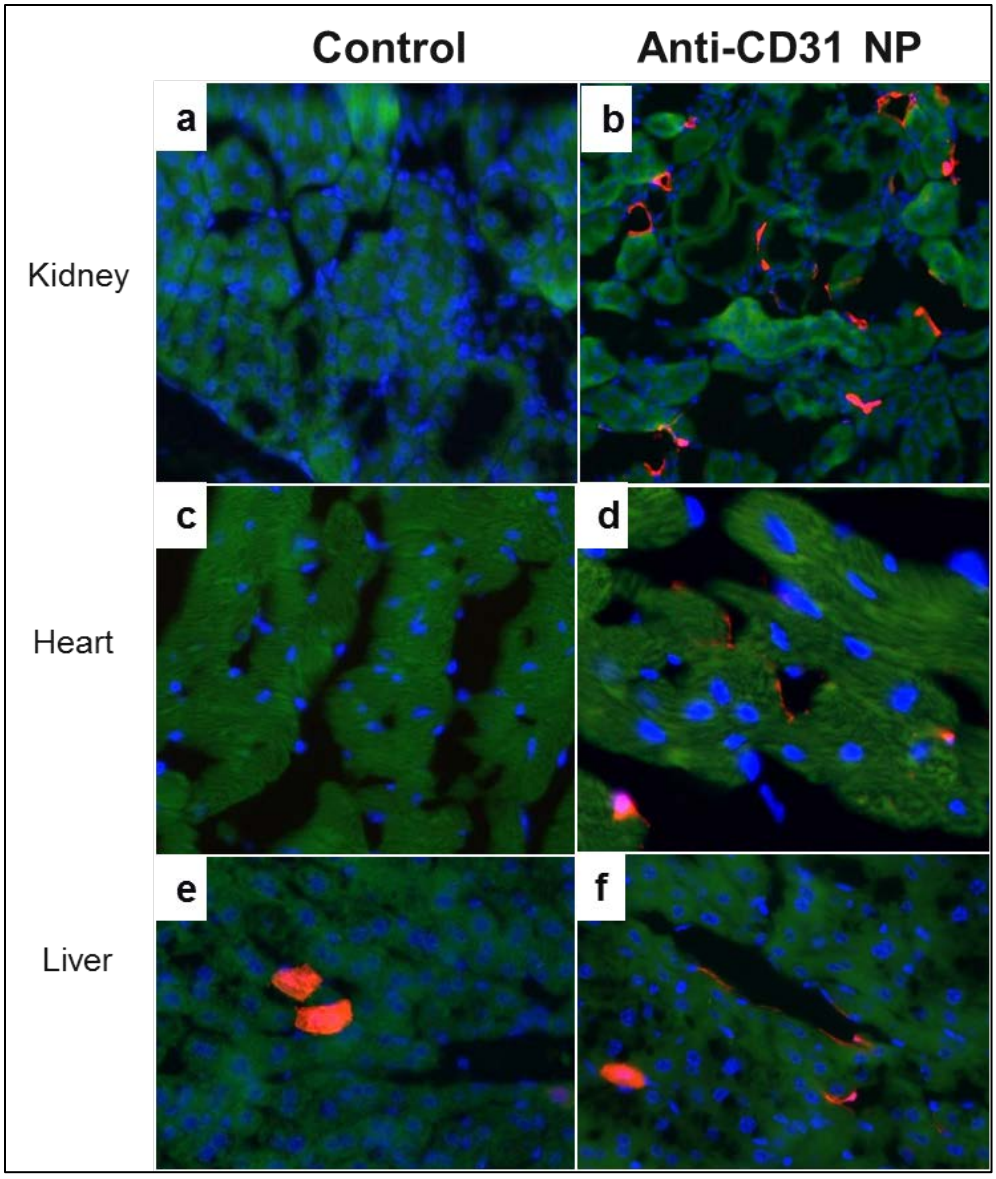


**Figure 2-16: Fluorescence microscopy of tissue sections after endothelial cell targeting of induced Cre recombination with anti-CD31 PLGA(50:50) OH-Tam-loaded nanoparticles.** In the control samples (nanoparticles without targeting antibody), no tdTomato expression in cells resembling endothelial cells is apparent. In mice injected with anti-CD31 targeted nanoparticles, clear vascular structures are apparent in multiple organ systems.

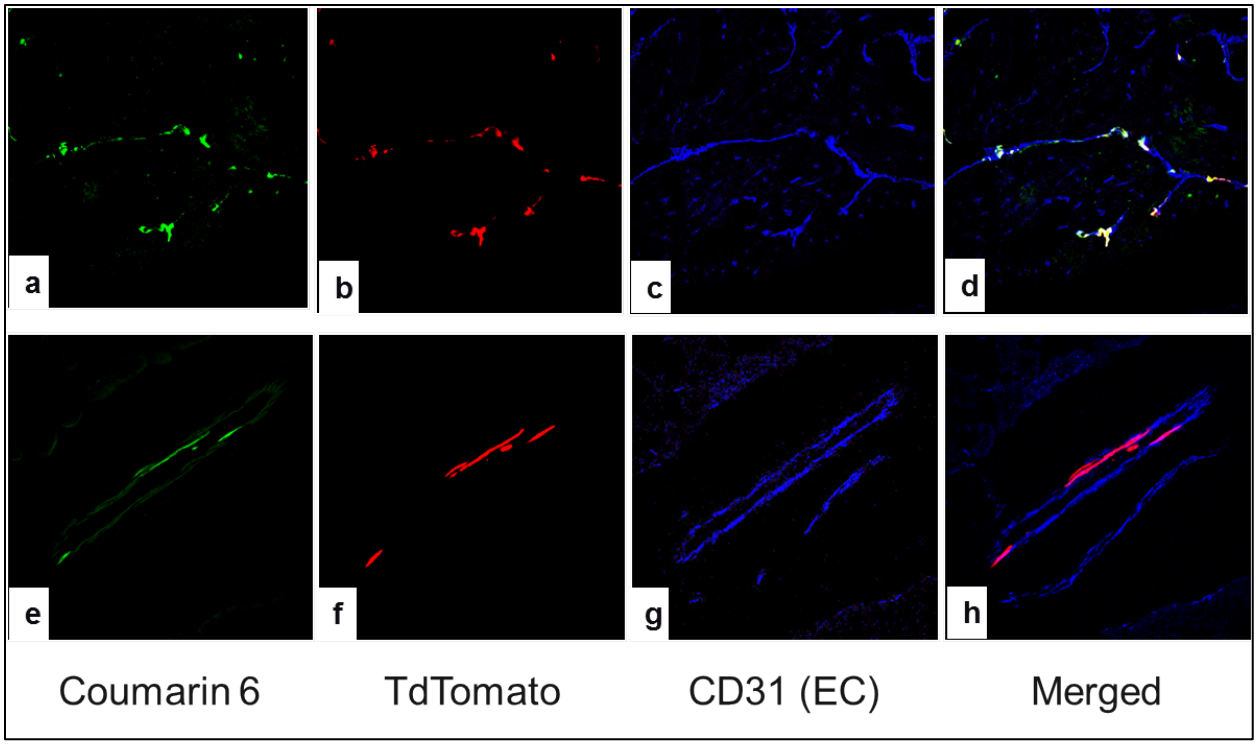


**Figure 2-17: tdTomato expression in endothelial cells following targeted OH-Tam delivery by anti-CD31 PLGA(50:50) nanoparticles.** These Confocal micrographs of two different representative areas (a-d) and (e-h) demonstrate clear co-localization of nanoparticles (Coumarin 6) and tdTomato gene expression in stained CD31+ endothelial cells.

In vivo targeting of anti-CD11b OH-Tam-loaded nanoparticles

The ability for anti-CD11b OH-Tam-loaded nanoparticles to enhance targeting to bloodstream monocytes and neutrophils was tested in the CreEr-tdTomato mouse model (Figures 2-18 and 2-19). FACS analysis for CD11b positive cells revealed that a distinct population of tdTomato positive cells did exist from the CD11b+ population. This would indicate that recombination had occurred. Blood from each mouse injected with nanoparticles was analyzed with FACS. All of the data was combined, and this revealed that the addition of CD11b antibody to the surface of the nanoparticle resulted in an almost 9-fold increase in the upake of nanoparticles in bloodstream CD11b+ (monocytes and neutrophils) cells.

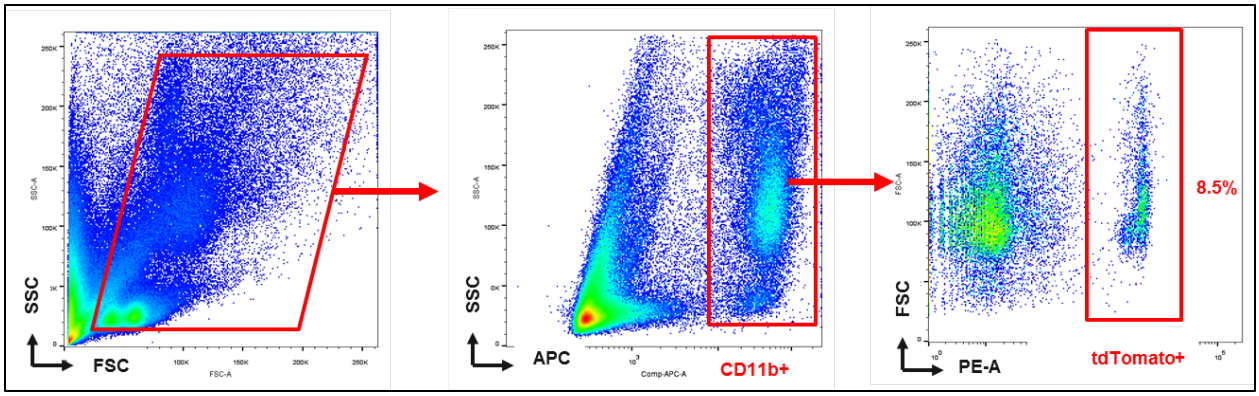


**Figure 2-18: FACS analysis of lysed blood from Rosa26CreER-tdTomato mice after targeting with anti-CD11b PLGA(50:50) OH-Tam-loaded nanoparticles.** This representative analysis demonstrates a distinct population of tdTomato+ cells from the CD11b+ population in which recombination has occurred, due to uptake of the targeted nanoparticles.

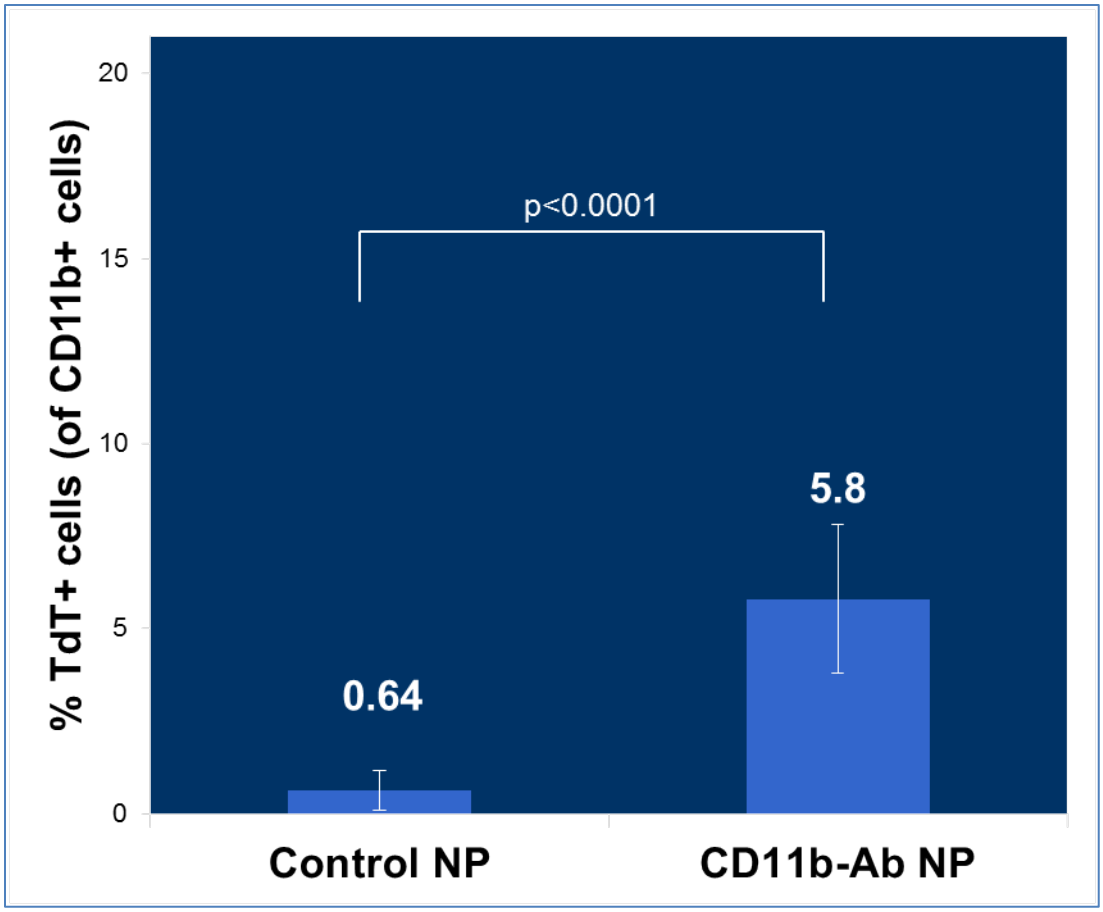


**Figure 2-19: Summary of FACS analysis data**. These data show a significantly increased (by over a factor of 9) percentage of CD11b+ cells that undergo recombination and express tdTomato after targeting targeting with anti-CD11b PLGA(50:50) OH-Tam-loaded nanoparticles.

## 2.4 DISCUSSION

These results demonstrate that the emulsification-solvent evaporation method can reliability and reproducibly create monodisperse formulations of PLGA nanoparticles encapsulating 4-Hydroxytamoxifen. These nanoparticles have been shown for the first time to induce gene recombination and reporter protein expression both *in vitro* and *in vivo*, in two different CreER/loxP systems. In addition, it was shown that the successful delivery of OH-Tam was based on direct nanoparticle uptake into the cell and release of the drug into the cytoplasm. This was confirmed with co-localization of particles with cells expressing the reporter protein, and verification that the nanoparticles do not release the OH-Tam into the bloodstream at detectable levels. Furthermore, it was demonstrated that targeting ligands could be added to the nanoparticles to preferentially increase nanoparticle uptake into the cell and tissue types of interest.

However, limitations remain with this system. As with most nanoparticle delivery systems reported in the literature, a significant amount of delivered nanoparticles becomes filtered out of the bloodstream by the mononuclear phagocyte system before the particles reach their intended destination. In addition, nanoparticles optimized for the delivery of OH-Tam (a very lipophilic molecule) do not necessarily make the best carriers for hydrophilic compounds such as proteins or nucleic acids, classes of molecules of significant therapeutic interest. Also, the conjugation reaction for attachment of antibody is not efficient for the consumption of antibody. These issues will need to be addressed prior to commercialization of this product.

# CHAPTER 3: NANOPARTICLE TARGETING OF ISCHEMIC MYOCARDIUM

## 3.1 INTRODUCTION

Myocardial ischemia-reperfusion injury remains a major unmet medical need in the field of Cardiology and a subject of intense therapeutic interest. Countless drugs have been studied for the alleviation of ischemia-reperfusion injury, but have always fallen short of clinical efficacy despite promising results at the pre-clinical level. While many explanations have been offered for these failures, a few of them involve technical limitations of drug delivery itself that may lend themselves to alternative drug delivery technologies such as nanoparticles. For instance, many drugs have short blood circulation or solubility, or may require such high doses to be efficacious that they result in significant systemic or off-target side effects. By packaging drugs in nanoparticle form, and engineering the characteristics of the nanoparticles themselves, it may be possible to increase drug circulation times, use less dose, target certain tissue, and control the release rate of the delivered drug.

This chapter of the dissertation establishes the experimental methods and results that demonstrate the feasibility of targeted nanoparticles for enhanced accumulation and drug delivery in myocardium subjected to ischemia reperfusion injury.

## 3.2 MATERIALS AND METHODS

### Materials

AlexaFluor 647-conjugated anti-mouse Ab (Cat# A-21239), AlexaFluor 647-conjugated anti-rat Ab (Cat# A-21472), AlexaFluor 647-conjugated anti-rabbit Ab (Cat# A-31573) were obtained from Life Technologies (Grand Island, NY).

α-actinin Ab (Cat# A7811) was obtained from Sigma-Aldrich (St. Louis, MO).

CD68 Ab (Cat# MCA1957T) was obtained from AbD Serotec (Kidlington, United Kingdom)

CD11b Ab (Cat# 553308) was obtained from BD Biosciences (Franklin Lakes, NJ)

CD31 Ab (Cat# ab2364) was obtained from Abcam (Cambridge, United Kingdom).

PDGFR-α Ab (Cat# sc-338) was obtained from Santa Cruz Biotechnology (Dallas, TX)

All other materials used were previously delineated in Section 2.2.

Mouse Ischemia-reperfusion injury model

Adult mice (both male and female) approximately 12-15 weeks old were subjected to myocardial ischemia-reperfusion injury through LAD ligation and release in the following manner. Briefly, the animals were anesthetized with 1-3% isoflurane and intubated through the trachea. The heart was exposed through lateral thoracotomy. Ligation of the left anterior descending artery was then performed. After 45 minutes of occlusion, the suture was released. The chest was then closed and sutured, and the animals allowed to recover on a heating pad. Per each specific study protocol, nanoparticles were injected either directly into the injury zone, or through a lateral tail vein at the specified time point. At the indicated time points, the mice were then euthanized by cervical dislocation after anesthesia with 5% isoflurane. Heparin was injected prior to anesthesia to prevent coagulation of blood in the coronary arteries. The hearts were harvested, and cleaned by clamping and ligating the aorta to a 22G needle cannula, and running cold PBS solution through the cannula. The hearts were then fixed in 4% paraformaldehyde overnight at 4ºC, followed by dehydration with sucrose solution for 24 hours. The hearts were then mounted in OCT embedding compound (Tissue-Tek), and frozen at -80ºC for 48 hours. Sections of 6-8μm

thick tissue in a transverse orientation were then cut with a cryostat, and mounted on standard histological slides. Analysis of sections was as protocol below.

*In vivo* study of OH-Tam-loaded nanoparticle uptake in injured myocardium

The distribution and accumulation of OH-Tam-loaded nanoparticles in the injured and non-injured regions of the heart after ischemia-reperfusion injury was studied in the $Rosa26^{CreER};tdT^{F/F}$ transgenic mouse model. Briefly, OH-Tam nanoparticles were first generated as previously described. $Rosa26^{CreER};tdT^{F/F}$ mice then underwent ischemia-reperfusion cardiac injury as described above. 400 μg of nanoparticles were injected into the lateral tail vein at either 1, 4, or 24 hours after reperfusion. As a control, 2 mice underwent direct injection of nanoparticles into the border zone of the injured region. After 7 days, the mice were euthanized by cervical dislocation after anesthesia with 5% isoflurane. Heparin was injected prior to anesthesia to prevent coagulation of blood in the coronary arteries. For each mouse, the heart was harvested. The heart was then fixed in 4% paraformaldehyde overnight at 4ºC, followed by dehydration with sucrose solution for 24 hours. The organs were then mounted in OCT embedding compound, and frozen at -80ºC for 48 hours. Sections of 6-8μm thick tissue were then cut in a transverse orientation with a cryostat, and mounted on standard histological slides. Imaging was then performed under fluorescence microscopy (AF6000LX, Leica Microsystems, Wetzlar, Germany)

In vivo study of anti-CD11b OH-Tam-loaded nanoparticle targeting of ischemic myocardium

Targeting of ischemia by anti-CD11b OH-Tam-loaded nanoparticles was studied in the $Rosa26^{CreER};tdT^{F/F}$ transgenic mouse model. Briefly, anti-CD11b-conjugated nanoparticles were prepared as described above. As a control, OH-Tam-loaded nanoparticles that did not undergo

any antibody conjugation were also prepared. Rosa26$^{CreER}$;tdT$^{F/F}$ mice then underwent ischemia-reperfusion cardiac injury as described above. For each of these conditions, 900 μg of conjugated nanoparticles (300 μg for 3 consecutive days) were injected into the lateral tail vein of the mice. After the fourth day, the mice were then euthanized by cervical dislocation after anesthesia with 5% isoflurane. Heparin was injected prior to anesthesia to prevent coagulation of blood in the coronary arteries. For each mouse, the heart, one lung, one kidney, the liver, and the spleen, were harvested. The organs were then fixed in 4% paraformaldehyde overnight at 4ºC, followed by dehydration with sucrose solution for 24 hours. The organs were then mounted in OCT embedding compound, and frozen at -80ºC for 48 hours. Sections of 7-8μm thick tissue were then cut with a cryostat, and mounted on standard histological slides. Immunofluorescent staining on the frozen sections was performed using a primary antibody to CD68, CD31, PDGFR-α, α-actinin, and the appropriate AlexaFluor 647-conjugated secondary antibody (Life). Imaging was then performed under fluorescence microscopy (AF6000LX, Leica Microsystems, Wetzlar, Germany) as well as confocal microscopy (TCS SP5-STED, Leica Microsystems, Wetzlar, Germany).

## 3.3 RESULTS

*In vivo* study of OH-Tam-loaded nanoparticle uptake in injured myocardium

The ability to distinguish areas of injury was first assessed by subjecting a mouse to LAD ligation ischemia-reperfusion injury, followed by cross-sectioning of the heart at the area of LAD ligation (Figure 3-1). It is readily apparent from fluorescent microscopy that areas of injury lose their natural auto-fluorescence and thus are easily identified. This gives us then the ability to separate study and analyze the regions of injury in comparison to control regions.

The accumulation of OH-Tam-loaded PLGA(50:50) in areas of ischemia-reperfusion injury was then investigated in the CreER-tdTomato transgenic mouse model (Figure 3-2). After tail vein injection of the nanoparticles in mice that had been subjected to LAD ligation and release, the areas of ischemia-reperfusion injury were analyzed under fluorescence microscopy for tdTomato expression, and compared to control regions in the heart that did not show signs of injury. It can be seen that many positive cells are present in the areas of injury, whereas no positive cells can be seen in the control non-injured regions. This would indicate that more nanoparticle uptake and accumulation occurred in the areas of ischemia-reperfusion injury, resulting in more cell recombination and expression of tdTomato.

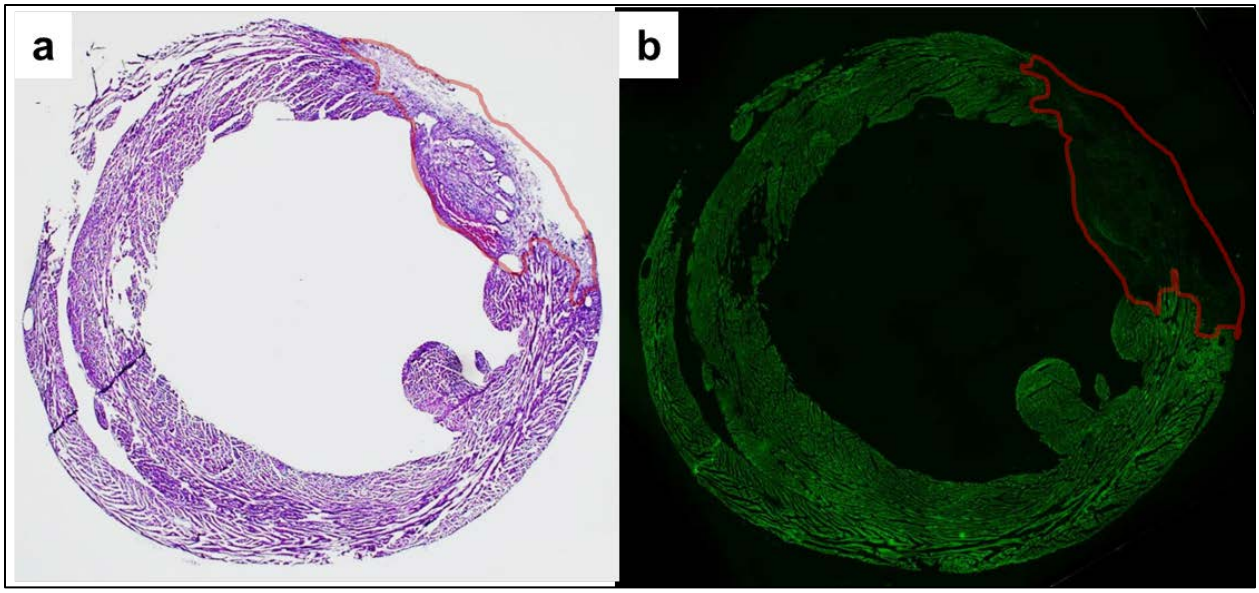


**Figure 3-1: Cross-sectional microscopy of heart after ischemia-reperfusion injury.** The area of injury (demarcated in red) is clearly seen in both the H&E stain (a) and the fluorescent micrograph (b) showing decrease in cardiac myocardium auto-fluorescence (in the GFP channel) in the area of injury.

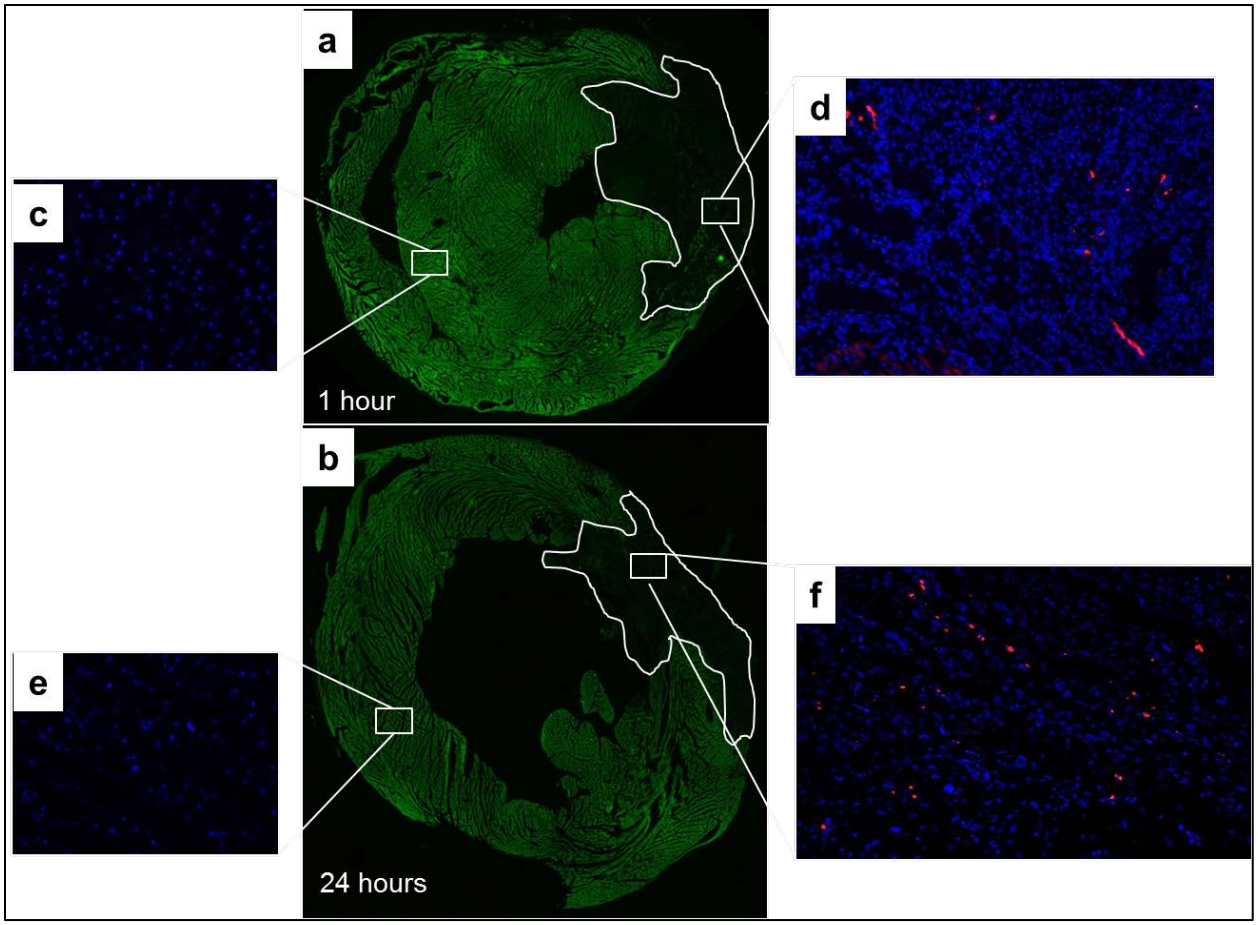


**Figure 3-2: Increase in nanoparticle uptake in regions of ischemia-reperfusion injury.** Panels (a) and (b) are representative heart cross sections under fluorescent microscopy showing clear areas of injury, in which PLGA(50:50) OH-Tam loaded nanoparticles were injected in the lateral tail vein either 1 hour or 24 hours after injury respectively. Panels (d) and (f) are representative fluorescent micrographs taken within the regions of injury, showing many cells that have undergone nanoparticle uptake with resulting recombination. Panels (c) and (e) are representative fluorescent micrographs taken in areas of normal myocardium, showing absence of cells that have undergone recombination.

In vivo study of anti-CD11b OH-Tam-loaded nanoparticle targeting of ischemic myocardium

The ability to further increase nanoparticle drug delivery to regions of cardiac ischemic injury through attachment of a targeting ligand was investigated using anti-CD11b PLGA(50:50) OH-Tam-loaded nanoparticles in the Rosa26CreER-tdTomato transgenic mouse model (Figure 3-3). It was hypothesized that the accumulation of macrophages and neutrophils as part of the standard inflammatory response to ischemia-reperfusion injury would provide a natural epitope-rich target for the nanoparticles. In targeting circulating monocytes and neutrophils (in addition to macrophages already present in the injury region), the nanoparticles could potentially be picked up by cells while in the bloodstream, and carried to the site of injury by the inflammatory cell.

Figure 3-3a shows a cross section under fluorescence microscopy. Even under low magnification it is apparent that the injured region contains a great deal of positive recombined cells. These cells, specifically in the border region with uninjured tissue, were analyzed under Confocal microscopy. This revealed that the tdTomato positive cells (Figure 3-3c) co-localized with Coumarin 6 (Figure 3-3b), and stained positive for CD68 (Figure 3-3d), indicating successful targeting of macrophages/monocytes by the nanoparticles.

In another cross section (Figure 3-4), there appeared to be a large cluster of cells that on fluorescence microscopy resembled cardiomyocytes rather than macrophages. This was further analyzed on Confocal microscopy, and confirmed to be cardiomyocytes by staining for cardiomyocyte marker α-actinin (Figure 3-4d). In addition, these cells also showed co-localization of Coumarin 6 (Figure 3-4c), indicating that the nanoparticles, while targeted to macrophages, actually did eventually reach the cardiac parenchymal tissue. While this finding was present in only one of the mice tested in this experiment, it provides evidence that this

targeting strategy may potentially allow delivery of therapeutics to cardiomyocytes even if targeted to other cell types.

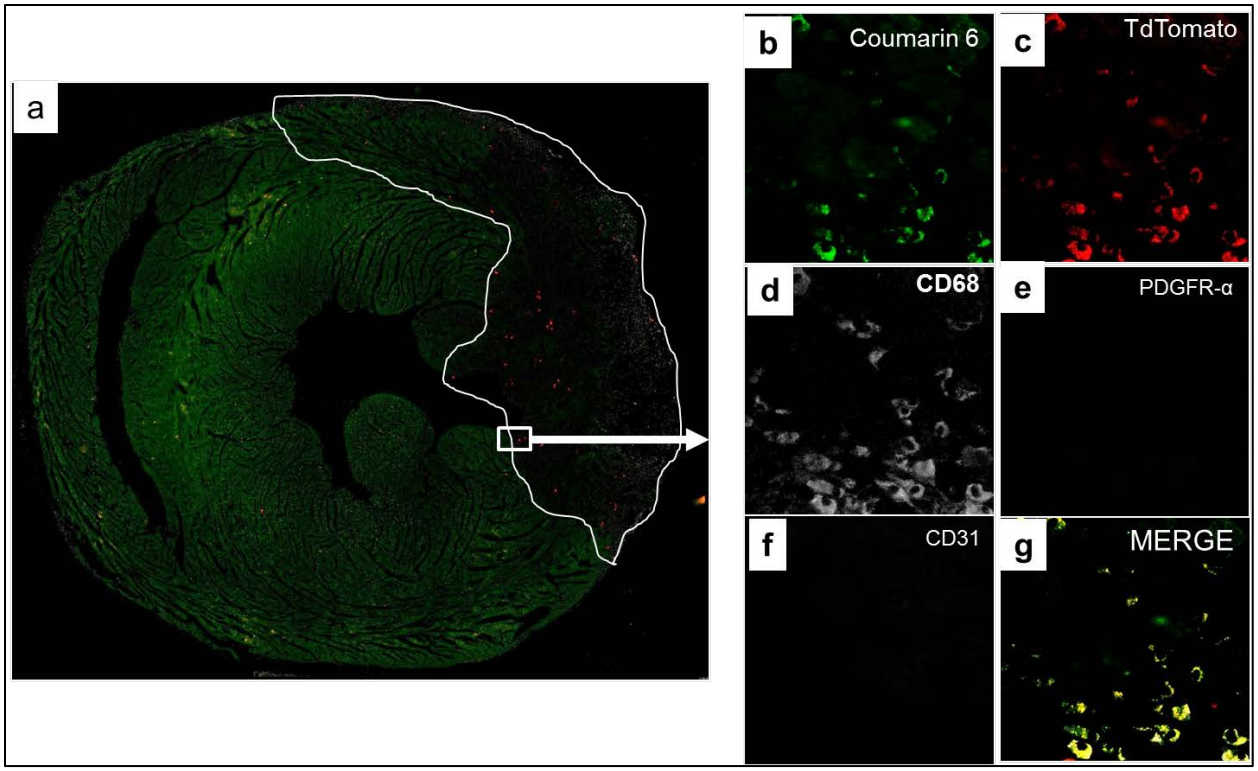


**Figure 3-3: Increase in nanoparticle uptake in area of ischemia-reperfusion injury after targeting with anti-CD11b PLGA(50:50) OH-Tam-loaded nanoparticles.** Panel (a) is a representative heart cross section under fluorescent microscopy showing clear area of injury. Of note, many cells are visible in the ischemic region that have undergone recombination, a finding not present at this magnification in the experiment shown in Figure 3-2 using non-targeted nanoparticles. Confocal microscopy (b-g) demonstrates that the tdTomato positive cells are CD68+ macrophages.

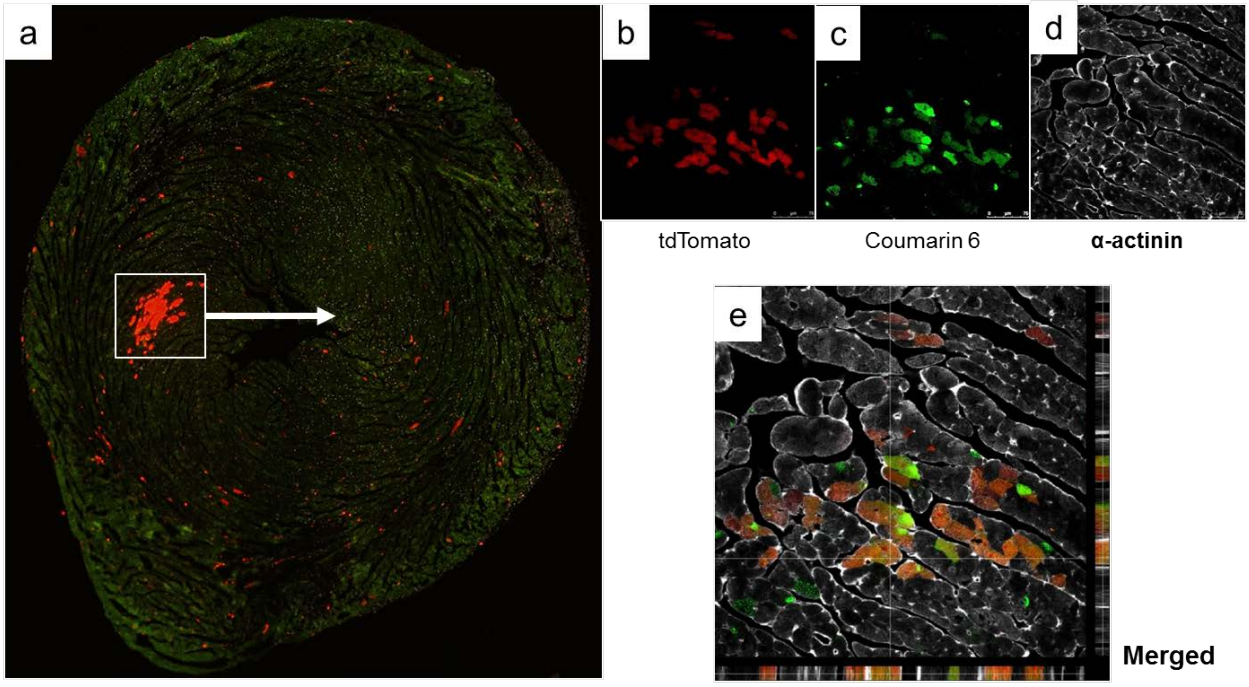


**Figure 3-4: Cardiomyocyte uptake of targeted anti-CD11b PLGA(50:50) OH-Tam-loaded nanoparticles in vivo.** Panel (a) is a heart cross section (near the heart apex) under fluorescent microscopy showing clear injury throughout the field of view as well as numerous tdTomato+ cells that have undergone recombination. There is a large cluster of cells in this view that appear to be cardiomyocytes in morphology. Confocal microscopy (b-e) confirms that the cluster of tdTomato+ cells are.α-actinin+ cardiomyocytes.

## 3.4 DISCUSSION

These results demonstrate for the first time that nanoparticle accumulation and drug delivery to cardiac tissue (of OH-Tam, as evidenced by reporter protein expression) is increased in regions of ischemia-reperfusion injury. This may be a result of increased nanoparticle extravasation into the sites of injury due to damage of the capillary endothelium, a known pathological complication of ischemia-reperfusion injury. In addition, it was shown for the first time that nanoparticle accumulation and drug delivery to cardiac tissue can be increased by targeting the nanoparticles to macrophages, a cell type that is well known to accumulate in regions of inflammation and injury. Furthermore, it was shown that targeting the nanoparticles to macrophages can actually enable nanoparticle uptake and drug delivery into cardiomyocytes at the region of injury. This was an unexpected result, and may be due to increase in the local concentration of nanoparticles from macrophage accumulation/processing and exocytosis into the surrounding environment. Taken together, these findings offer a roadmap for rational development of improved nanoparticle systems for delivery of therapeutic agents to areas of ischemia-reperfusion injury.

However, many questions still remain. The relationship between the degree of ischemia-reperfusion injury / capillary endothelial disruption and the enhanced permeability to nanoparticles is incompletely understood; the time course of increased permeability and the size boundaries remain unknown. It is also unknown whether there is also a concurrent change in the drainage system of the injured region, that is, whether extravasated nanoparticles may be subject to either increased or decreased clearance from the injured region. This would play a major role on the kinetics of nanoparticle accumulation and intracellular uptake. Finally, more work needs

to be done to determine the ideal ligand/epitope to use to improve nanoparticle targeting to the injured myocardium.

# CHAPTER 4: ENHANCED NANOPARTICLE UPTAKE THROUGH MODIFICATION OF VASCULAR PERMEABILITY

## 4.1 INTRODUCTION

The homeostatic intact endothelial cell lining functions as a major barrier to the passage of nanoparticles into the interstitial space of tissues. Indeed, the success of many cancer nanoparticle-based therapeutics has relied on the EPR effect resulting from the disruption of a healthy intact endothelial barrier. Bioengineering strategies to improve drug delivery across the blood brain barrier have included use of nonthermal focused ultrasound coupled with intravenous injection of microbubbles, which then cavitate when activated by the ultrasound pulses and transiently opens tight junctions in the endothelial lining. Part of the natural biological regulation of endothelial permeability includes chemical mediators of increased permeability in conditions of inflammation, including histamine, bradykinin, serotonin, nitric oxide, and prostaglandins. It is hypothesized that controlling the local vascular permeability of a tissue can influence nanoparticle uptake and drug delivery.

This chapter of the dissertation establishes the experimental methods and results that demonstrate the feasibility of controlling vascular permeability through chemical mediators in order to enhance nanoparticle uptake and distribution in various tissues and organs.

## 4.2 MATERIALS AND METHODS

### Materials

Histamine bisphosphate monohydrate (Cat# 53310) was obtained from Sigma-Aldrich (St. Louis, MO).

All other materials used were previously described in Section 2.2.

Effect of histamine on NP uptake

The effect of histamine on NP tissue uptake and resulting organ distribution was studied in the $Rosa26^{CreER};tdT^{F/F}$ transgenic mouse model. Briefly, OH-Tam loaded nanoparticles were prepared as described previously. 500mg of nanoparticles along with 4mg of Histamine were injected into the lateral tail vein of $Rosa26^{CreER};tdT^{F/F}$ transgenic mice daily for 2 consecutive days.. As a control, other mice underwent injection of nanoparticles without any Histamine. After 3 days, the mice were euthanized by cervical dislocation after anesthesia with 5% isoflurane. Heparin was injected prior to anesthesia to prevent coagulation of blood in the coronary arteries. All experimental samples were generated in triplicate. For each mouse, the heart, one lung, one kidney, the liver, and the spleen, were harvested. The organs were then fixed in 4% paraformaldehyde overnight at 4ºC, followed by dehydration with sucrose solution for 24 hours. The organs were then mounted in OCT embedding compound, and frozen at -80ºC for 48 hours. Sections of 7-8μm thick tissue were then cut with a cryostat, and mounted on standard histological slides. Imaging was then performed under fluorescence microscopy (AF6000LX, Leica Microsystems, Wetzlar, Germany). 3 sections per organ were imaged, with micrographs taken of 5 20x fields per section. Quantification of cells in each image was performed using ImageJ image processing and analysis software (NIH). Numerical results are presented as the number of positive recombined cells per field of view, normalized to control ± standard deviation. Statistical testing was performed using the Student's t-test, and statistical significance was achieved with a two-sided $P$ value $\leq 0.05$.

## 4.3 RESULTS

Effect of histamine on NP uptake

Figure 4.1 illustrates representative fluorescence microscope images of organ sections in mice injected with OH-Tam-loaded PLGA(50:50) nanoparticles and with/without histamine. It can be appreciated that there is a mild decrease in the number of positive cells in the liver and spleen with histamine administration, and a mild increase in the number of positive cells in the other organs. Statistical analysis of the number of positive cells for each condition, as performed, and results are normalized to the number of positive cells in the control conditions/organs. There is a significant increase in the number of positive recombined cells seen in the heart (2.75x), kidney (6.14x), and lung (1.87x) with histamine co-administration with OH-Tam-loaded PLGA(50:50) nanoparticles. In contrast, there is a significant decrease in nanoparticle uptake and number of positive recombined cells in the liver (0.61x) and spleen (0.65). This is consistent with a decreased number of particles available for clearance by the liver and spleen with increased uptake by the other organs

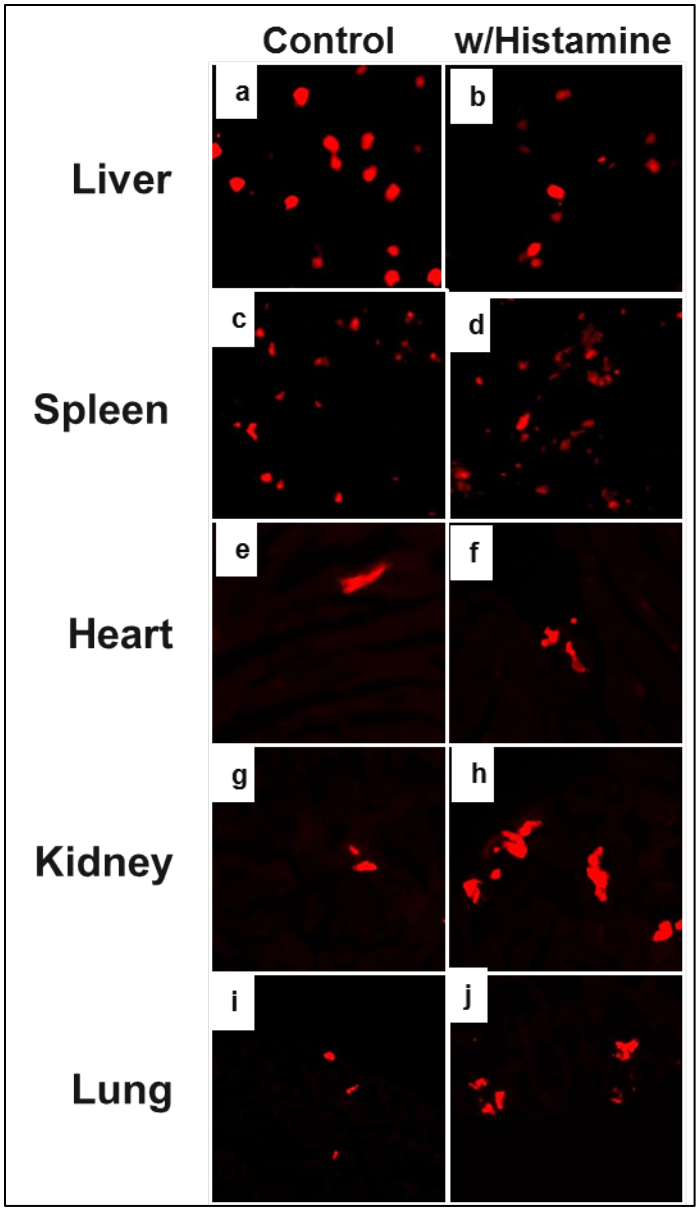


**Figure 4-1: Representative fluorescent micrographs of organ sections after OH-Tam-loaded PLGA(50:50) nanoparticles were injected with and without histamine.** A mildly appreciable decrease in the quantity of positive recombined cells can be seen in the liver (a-b) and spleen (c-d) micrographs, which a mildly appreciable increase in the quantity of positive recombined cells can be seen in the heart (e-f), kidney (g-h), and lung (i-j).

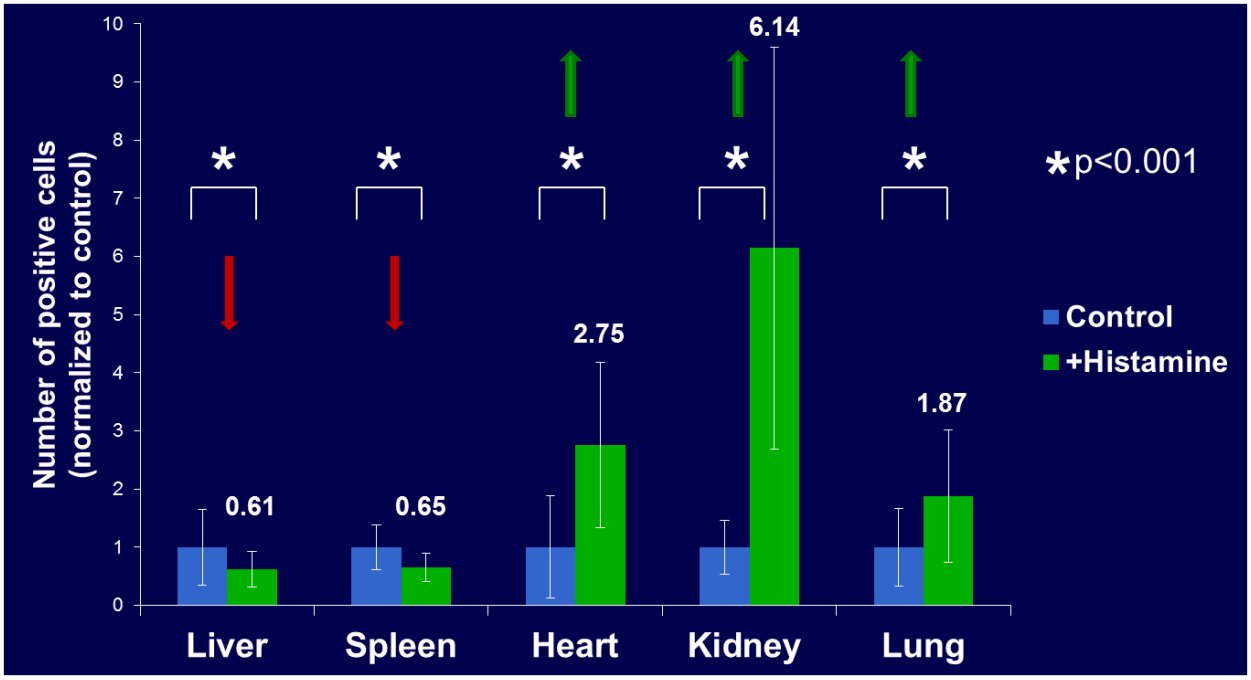


**Figure 4-2: Effect of histamine on the distribution of nanoparticle uptake in various organs.** Results are normalized to control. There is a significant increase in the number of positive recombined cells seen in the heart (2.75x), kidney (6.14x), and lung (1.87x) with histamine co-administration with OH-Tam-loaded PLGA(50:50) nanoparticles. In contrast, there is a significant decrease in nanoparticle uptake and number of positive recombined cells in the liver (0.61x) and spleen (0.65). This is consistent with a decreased number of particles available for clearance by the liver and spleen with increased uptake by the other organs.

## 4.4 DISCUSSION

These results demonstrate for the first time that histamine can be used as an agent to increase vascular permeability in order to increase nanoparticle uptake in specific organs and tissues of interest. It was shown that increasing vascular permeability through systemic injection of histamine resulted in greater nanoparticle uptake and drug delivery to many organs including the heart, kidney, and lung. In doing so, less of the administered nanoparticles were cleared by the liver and spleen, resulting in a more favorable biodistribution of nanoparticles. This strategy can be further investigated to determine the best vasoactive mediator for local drug delivery. Control of vascular permeability through focused ultrasound, in conjunction with chemical mediators, may be another option to improve nanoparticle uptake into tissues.

# CHAPTER 5: CONCLUSIONS AND FUTURE DIRECTIONS

## 5.1 LIST OF NOVEL FINDINGS

Nanoparticles for tissue-specific inducible Cre recombination

- Gene recombination in inducible Cre mice can be spatially adjusted by packaging 4-Hydroxytamoxifen in NP form
- Tissue specificity of gene recombination in inducible Cre mice can be enhanced through tissue targeting of NP, even with CreER under the control of a universal promoter

Nanoparticles for drug delivery to ischemic myocardium

- Nanoparticle uptake is increased in cardiac tissue subjected to ischemia-reperfusion injury
- Nanoparticle uptake in injured cardiac tissue can be enhanced through macrophage targeting
- Nanoparticle uptake in cardiac tissue can be increased by controlling vascular permeability

## 5.2 CONCLUSIONS

This research has demonstrated the feasibility of using direct nanoparticle encapsulation and delivery of 4-Hydroxytamoxifen into cells to induce gene recombination in transgenic CreER-loxP mice. This was done using a PLGA(50:50)/OH-Tam nanoparticle system which could be engineered to display a surface-conjugated antibody for tissue specific targeting. The induced recombination was found to be due to intracellular direct delivery of OH-Tam by the nanoparticle. Recombination could significantly increased in specific cell types by attachment of

a targeting ligand. Specifically with myocardial ischemia-reperfusion injury, it was found that nanoparticle uptake was increased in areas of injury, and this uptake could be increased by attachment of a targeting ligand to macrophages. Finally control of vascular permeability can be used to influence tissue uptake and biodistribution of nanoparticles.

## 5.3 THERAPEUTIC OPTIONS

A large number of pharmacological agents studied have been shown to reduce infarct size in animal models of ischemia-reperfusion injury [22]. These include adenosine, cyclosporine, erythropoietin, nicorandil, and atrial natriuretic peptide. However, clinical trial results involving these agents have been mixed. While many reasons for the disappointing translation of pre-clinical research to clinical results are likely, some of the potential reasons involve the lower bioavailability of traditionally administered therapeutics when compared to newer bioengineered controlled release and targeted formulations. One of the most promising candidates for minimizing ischemia-reperfusion injury has been cyclosporine [23]. It is a potent inhibitor of the mitochondrial permeability transition pore (an important determinant of reperfusion injury) and has been studied in pilot clinical trials to decrease infarct size and improve left ventricular function when administered at the time of acute reperfusion [24,25]. A phase III randomized clinical trial was recently initiated to evaluate the clinical efficacy of cyclosporine in reducing the 1-year composite of mortality, rehospitalization, and left ventricular remodeling when given at the time of primary PCI. As with all of the previously tested therapies, it remains to be seen whether cyclosporine can continue its initial promising results from pre-clinical and pilot clinical studies. As a poorly soluble hydrophobic molecule, it necessitates packing within a lipid emulsion for proper injection and administration. This brings up the possibility that its bioavailability within the injured myocardial tissue may not be sufficient for adequate clinical

benefit. As such, it would make an ideal candidate for packaging in nanoparticle form for targeted delivery to injured tissue and controlled release from a nanoparticulate carrier.

## 5.4 FUTURE DIRECTIONS

Potential future directions fall into three main categories: improving tissue specificity of nanoparticles, developing improved experimental tools, and better understanding and controlling vascular permeability for the purposes of nanoparticle delivery.

To improve tissue specificity, more work needs to be done first on reducing natural bloodstream clearance of nanoparticles by the mononuclear phagocyte system. This may potentially include modifications to the nanoparticles to be more “stealthy”, such as with the addition of PEG. More targeting ligands need to be investigated, to determine the optimum type and epitope for a specific tissue of interest.

Experimental tools that would advance the field include development of nanoparticle systems able to co-deliver hydrophobic as well as hydrophilic molecules. This would enable a greater range of applications for nanoparticle diagnostics and therapeutics. In addition, the induced Cre transgenic mouse model would benefit greatly from the use of a “library” of OH-Tam-loaded nanoparticles, each with a different targeting ligand to a certain tissue of interest. In this manner, tissue specific recombination could be induced with Cre under the control of a ubiquitous promoter rather than a tissue specific promoter. This would potentially save up to years and tens of thousands of dollars in development costs for a particular mouse strain.

Finally, the field would be greatly advanced by methods for better controlling vascular permeability in order to control nanoparticle uptake. This may involve development of better

ultrasound technologies as well as more experimental modeling of the ultrasound parameters relevant to controlling permeability.

## BIBLIOGRAPHY


1. **Mozaffarian D, Benjamin EJ, Go AS, *et al.*** Heart disease and stroke statistics--2015 update: a report from the American Heart Association. *Circulation*. 2015; 131: e29-322.
2. **Yellon DM, Hausenloy DJ.** Myocardial reperfusion injury. *The New England journal of medicine*. 2007; 357: 1121-35.
3. **Chen J, Normand SL, Wang Y, *et al.*** National and regional trends in heart failure hospitalization and mortality rates for Medicare beneficiaries, 1998-2008. *JAMA : the journal of the American Medical Association*. 2011; 306: 1669-78.
4. **Yancy CW, Jessup M, Bozkurt B, *et al.*** 2013 ACCF/AHA guideline for the management of heart failure: a report of the American College of Cardiology Foundation/American Heart Association Task Force on Practice Guidelines. *Journal of the American College of Cardiology*. 2013; 62: e147-239.
5. **Hausenloy DJ, Yellon DM.** Myocardial ischemia-reperfusion injury: a neglected therapeutic target. *The Journal of clinical investigation*. 2013; 123: 92-100.
6. **Nabel EG, Braunwald E.** A tale of coronary artery disease and myocardial infarction. *The New England journal of medicine*. 2012; 366: 54-63.
7. **Milavetz JJ, Giebel DW, Christian TF, *et al.*** Time to therapy and salvage in myocardial infarction. *Journal of the American College of Cardiology*. 1998; 31: 1246-51.
8. **Andersen HR, Nielsen TT, Rasmussen K, *et al.*** A comparison of coronary angioplasty with fibrinolytic therapy in acute myocardial infarction. *The New England journal of medicine*. 2003; 349: 733-42.
9. **Hillis LD, Smith PK, Anderson JL, *et al.*** 2011 ACCF/AHA Guideline for Coronary Artery Bypass Graft Surgery: executive summary: a report of the American College of Cardiology Foundation/American Heart Association Task Force on Practice Guidelines. *Circulation*. 2011; 124: 2610-42.
10. **Kamaly N, Xiao Z, Valencia PM, *et al.*** Targeted polymeric therapeutic nanoparticles: design, development and clinical translation. *Chemical Society reviews*. 2012; 41: 2971-3010.
11. **Makadia HK, Siegel SJ.** Poly Lactic-co-Glycolic Acid (PLGA) as Biodegradable Controlled Drug Delivery Carrier. *Polymers*. 2011; 3: 1377-97.
12. **Weissenbock A, Wirth M, Gabor F.** WGA-grafted PLGA-nanospheres: preparation and association with Caco-2 single cells. *Journal of controlled release : official journal of the Controlled Release Society*. 2004; 99: 383-92.
13. **Panyam J, Zhou WZ, Prabha S, *et al.*** Rapid endo-lysosomal escape of poly(DL-lactide-co-glycolide) nanoparticles: implications for drug and gene delivery. *FASEB journal : official publication of the Federation of American Societies for Experimental Biology*. 2002; 16: 1217-26.
14. **Bertrand N, Wu J, Xu X, *et al.*** Cancer nanotechnology: the impact of passive and active targeting in the era of modern cancer biology. *Advanced drug delivery reviews*. 2014; 66: 2-25.
15. **Matsumura Y, Maeda H.** A new concept for macromolecular therapeutics in cancer chemotherapy: mechanism of tumoritropic accumulation of proteins and the antitumor agent smancs. *Cancer research*. 1986; 46: 6387-92.
16. **Lee RJ, Fang Q, Davol PA, *et al.*** Antibody targeting of stem cells to infarcted myocardium. *Stem cells*. 2007; 25: 712-7.

17. **Lum LG, Fok H, Sievers R, *et al.*** Targeting of Lin-Sca+ hematopoietic stem cells with bispecific antibodies to injured myocardium. *Blood cells, molecules & diseases*. 2004; 32: 82-7.
18. **Dvir T, Bauer M, Schroeder A, *et al.*** Nanoparticles targeting the infarcted heart. *Nano letters*. 2011; 11: 4411-4.
19. **Gunschmann C, Chiticariu E, Garg B, *et al.*** Transgenic mouse technology in skin biology: inducible gene knockout in mice. *The Journal of investigative dermatology*. 2014; 134: e22.
20. **Zhang J, Zhao J, Jiang WJ, *et al.*** Conditional gene manipulation: Cre-ating a new biological era. *Journal of Zhejiang University Science B*. 2012; 13: 511-24.
21. **Plumb RS, Warwick H, Higton D, *et al.*** Determination of 4-hydroxytamoxifen in mouse plasma in the pg/mL range by gradient capillary liquid chromatography/tandem mass spectrometry. *Rapid communications in mass spectrometry : RCM*. 2001; 15: 297-303.
22. **Morel O, Perret T, Delarche N, *et al.*** Pharmacological approaches to reperfusion therapy. *Cardiovascular research*. 2012; 94: 246-52.
23. **Heusch G.** Cardioprotection: chances and challenges of its translation to the clinic. *Lancet*. 2013; 381: 166-75.
24. **Piot C, Croisille P, Staat P, *et al.*** Effect of cyclosporine on reperfusion injury in acute myocardial infarction. *The New England journal of medicine*. 2008; 359: 473-81.
25. **Mewton N, Croisille P, Gahide G, *et al.*** Effect of cyclosporine on left ventricular remodeling after reperfused myocardial infarction. *Journal of the American College of Cardiology*. 2010; 55: 1200-5.